Dear Editor,

Thank you for considering our manuscript for publication. Below you find the replies to the referees followed by the marked-up manuscript. Our replies to the referees are in blue and lines numbers refer to related changes in the manuscript. Changes in the manuscript are in red. Please note that all figures have been updated.

Kind regards,
Marcel Ricker

Reply to:

Interactive comment on "Circulation of the European Northwest Shelf: A Lagrangian perspective" by Marcel Ricker and Emil V. Stanev

Anonymous Referee #1
Received and published: 16 January 2020
Review of 'Circulation of the European Northwest Shelf: A Lagrangian perspective' by Marcel Ricker and Emil Stanev.

We thank reviewer #1 for the detailed and extensive review of our paper. We provide point-by-point answers in the attached pdf.

Summary
The manuscript describes a series of Lagrangian particle tracking experiments carried out to characterise the water circulation and the accumulation of hypothetical particles on the northwest European continental shelf. Particles were released at the surface and the bottom at the start of monthly runs for six different scenarios, mostly uniformly distributed over the area. Some scenarios were carried out over one year, others only for January. A property called 'density trend' is defined to analyse the resulting particle movements. The analysis consists mainly of differences of this 'density trend' between the model scenarios.

General comments
This is an interesting manuscript, with powerful visualisations, supported to a large extent by the newly introduced 'density trend'. However, after reading it, I am left mostly confused,

because important information is not supplied (or has escaped my attention), and choices are not motivated (while some of these choices are bound to affect the results). Moreover, the results and discussion section is rather long-winded, depends on visual comparison between figures (which will end up on different pages), and seems to jump unpredictably between figures in quite a few places. It is not clear to me how the particles (are allowed to) move in the vertical (vertical mixing seems to be absent or under-represented). For a number of figures, it is not clear if surface, bottom or e.g. depth-averaged values are presented. Also, I have doubts about the January temperature fields presented/used: the temperatures seem too high, and I am surprised by the magnitude of the spatial gradients in the North Sea. Validation of these is absent. Overall, I would recommend major revisions. I will provide more detailed comments below.

Authors: In the following we provide the missing information and explain the questionable choices. We hope that the changes we introduce contribute to a better understanding of the manuscript. We rearranged the order of the manuscript and of the experiments. A detailed comment on the vertical particle movement is given in the following paragraph. The model has been re-calibrated and a comparison of surface temperatures and satellite data is shown in the supplementary material. Hence, ALL figures have been updated. As suggested, the quantity “density trend (DT)” has been renamed to “normalised cumulative particle density (NCPD)”.

Vertical particle motion

Under well-mixed conditions, as may be expected in most of the North Sea in winter, I would expect neutrally buoyant particles (as simulated here?) to be mixed quickly in the vertical by turbulent mixing processes. That means that there should be little difference in the overall dispersal of surface and bottom-released particles; yet, these differences are so substantial in the simulation results that it seems that most particles did not leave the surface or bottom model layer. Were the particles tied to the surface or bottom layer (i.e. vertical velocities set to zero)? It does not seem so, because at some point in the manuscript up- and down-welling are addressed. Was the effect of turbulent mixing omitted? Why? If so, I’m not sure what the presented results mean/represent. If the effects of (vertical) turbulent mixing were included, checks need to be made to see if this was done correctly. This needs to be resolved and/or absolutely clear, otherwise this work cannot be published.

Authors: We made clear in the revised manuscript that the used Lagrangian techniques aim at giving a new view on velocity field in the North Sea. In other words, the paper is about velocity, not so much about turbulence. We do not analyse the propagation and mixing of particles. In our setup, particles released in NEMO are always advected in 3-D by (u,v,w). That is, the particles are neutrally buoyant (added in line 163-164) and can be interpreted as following the

pathways of water parcels (Blanke and Raynaud, 1997). Because we study the properties of the velocity field, additional horizontal and vertical turbulent mixing is not introduced for particle tracking. As a consequence, the presented analyses are analyses of velocity properties and not of the effects of mixing (added in line 83-84 and 163-164).

Nevertheless, in terms of T/S, the water column is well mixed in January, thus the model physics can be treated as correct. The specific properties of the velocity field explains the difference of NCPD at the surface and bottom.

Implementations of turbulent mixing in Lagrangian tracking is mostly done by random walk schemes. The effect of horizontal diffusion is shown in Fig. R.1.1. We want to emphasise that the implementation of horizontal (van Sebille et al., 2018) and, in particular, vertical diffusion (van Sebille et al., 2020) in particle tracking are ongoing scientific subjects.

van Sebille, E., Aliani, S., Law, K. L., Maximenko, N., Alsina, J., Bagaev, A., et al. (2020). The physical oceanography of the transport of floating marine debris. Environmental Research Letters. https://doi.org/10.1088/1748-9326/ab6d7d

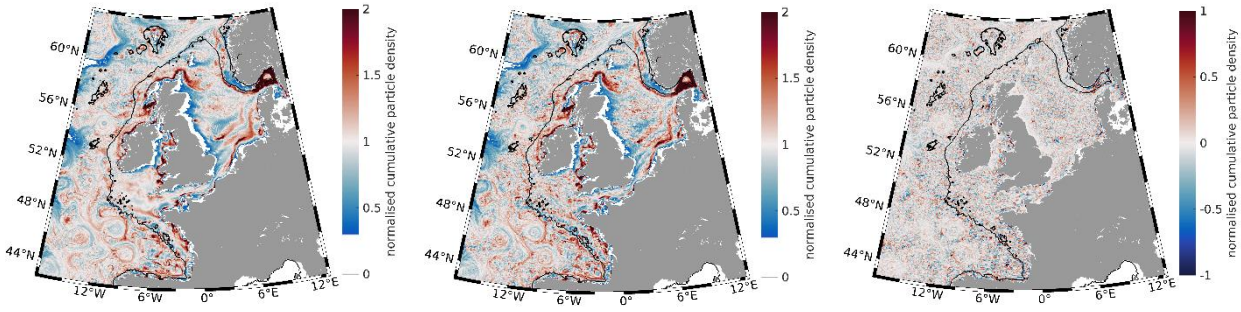

Fig. R1.1. Surface January 2015 NCPD without (left) and with (middle) additional horizontal diffusion in particle advection obtained from offline simulations. The right panel shows the difference without minus with diffusion.

Missing information (main points)

-It is not clearly explained a priory (section 2.4) why each experiment was carried out, and with which objective (what do you expect to learn and how will these experiments provide that knowledge)?

Authors: More details about the experiments and their objectives are added in the text (line 188-196).

-There is no validation of the temperature and salinity fields. The salinity fields correspond to what I would expect, but the temperature fields don't.

Authors: The model has been further tuned to better represent the thermohaline fields. A figure has been added in the supplementary material showing the RMSE of satellite and model data in January 2015 (Fig. S3; line 318-320).

-l. 54-62. Also discuss seasonal stratification and subsurface jets (eg. Hill ea 2008).

Authors: Seasonal stratification was already mentioned. Subsurface jets are referenced by citing Hill et al. (2008) (line 57-61).

-Different, and offline model for backtracking: a forward run of this model for the control run should be compared with CR to identify/quantify differences in results resulting from the model/method differences.

Authors: Such comparison has been made during the preparation of the manuscript and is mentioned in the text in line 151-153. The comparison in terms of NCPD using the results from

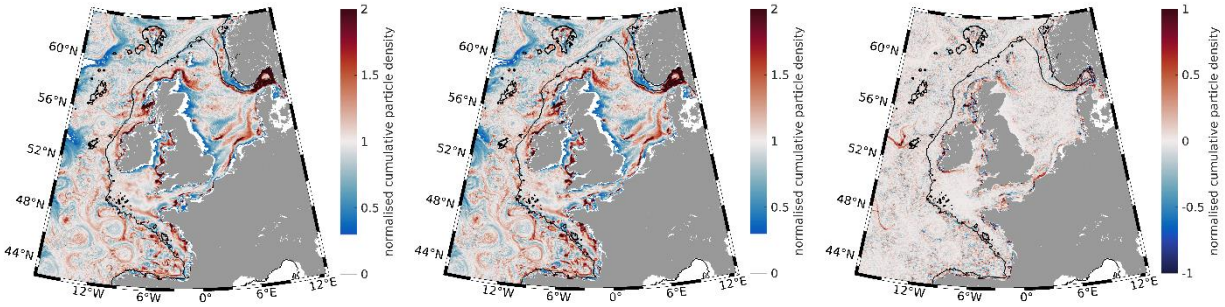

an online run without vertical advection and the same setup in OpenDrift for January 2015 is shown in Fig. R1.2 (NCPD online minus offline). The differences are rather minor.

Fig. R1.2. Surface January 2015 NCPD online 2-D (left), offline (middle) and the difference online minus offline (right).

-Markings in the figures (plusses, minuses, stars, arrows): It is not clear what the criteria were to place these where they were put (often other locations seem equally justifiable), or for which areas they hold. Please remove and find a different/better/more quantitative way to quantify/visualise/discuss this.

Authors: For Fig. 4, NCPD can be interpreted as a quantitative measure for particle accumulation. Thus, we decided to avoid any of these markers and we emphasise, that we describe examples of pronounced features (line 374-375 and 565).

-There is repeated mentioning of 'westerlies' as an explanation in the discussion/ conclusions, but no detail about the wind forcing is presented (e.g. to show that this was the dominant wind direction during the simulations), nor short-term simulations (e.g. to show what happens when the wind is from the west).

Authors: During the preparation of the manuscript, analyses of the wind have been made. To remove ambiguity also for other readers, a wind rose of these analyses has been added in the

supplementary material (Fig. S1; line 252-253). The wind contains (almost) always a western component.

-Section 3.4. Why were 80m intervals chosen? Why at these depths? Why allow gaps in the vertical in this analysis? What happens in the gaps? It would help if the initial positions were shown?

Authors: We are sorry about the confusion. There are no gaps. Particles are seeded every 20 m, i.e. at 1 m, 20 m, 40 m, … down to the bottom. Thus, the results in Fig. 9a are for the 1 m, 20 m, …, and 80 m seeding. The next seeding levels are 100 m, 120 m, …, and 180 m (Fig. 9b). So the gap in the labels is misleading and it should read 1-100 m, 100-200 m, 200-300 m and 900-1,000 m. An example of initial positions have been added in Fig. 9e. In the horizontal, the particles are seeded uniformly within the coloured area (1 per model grid).

-Figure 2: for which depths are these data presented? Surface, bottom, depthaveraged?

Authors: As given in the caption ("simulated surface properties"), the data is always shown for the surface (1 m) for the comparisons with surface NCPD.

-Monthly runs were done to depict DT. How dependent is the result on this monthly interval? For instance, what happens to the visualised results if 2 weeks or 2 months are used as interval?

Authors: 2 weeks and 2 months as integration time would lead to similar results (see Fig. R1.3; compare with Fig. 5a). In 2 weeks the results are noisier and accumulation areas less pronounced; 2 months already average out small-scale features. If the integration time is too long, vast areas show very low NCPD which results from "empty" grids that are no longer supplied by particles. For these grids (white grids in NCPD plots), the statistical relevance cannot be ensured.

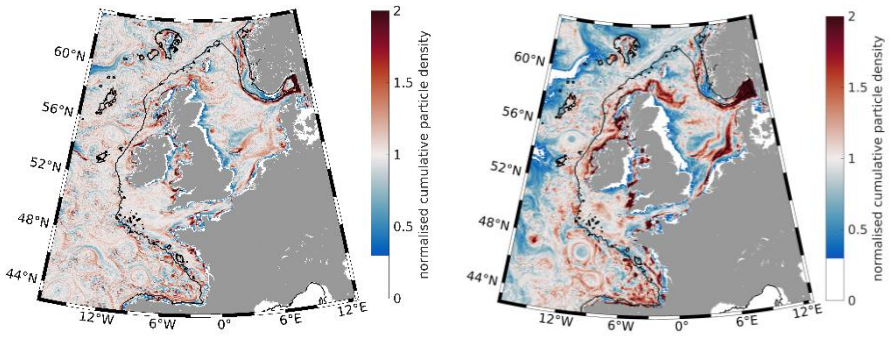

Fig. R1.3. Surface NCPD for the first 15 (left) and 60 days (right) in 2015.

Structure

-Section 2.2 contains results, please separate methods and results.

-Section 2.3 contains (many) results, please separate methods and results.

Authors: The results of Sect. 2.2 and 2.3 have been moved into the results (note the rearranged order of the manuscript).

-Results and discussion: there does not seem to be much system in the order in which the various release experiments (as in Table 2) are presented/discussed, with quite a few jumps between experiments. There also does not seem to be much balance in the amount of attention given to these various experiments. This makes it difficult for the reader to keep track of the narrative. This should be tidied up; one way of doing that would be to split the section into two separate Results and Discussion sections. Linking back to the objectives of each experiment (see also Missing information above) will also help here.

Authors: The structure of the manuscript has been revised. We tried to split the sections into equally long sections, whereas the balance between the experiments was not considerably changed, because some experiments require more attention (e.g. CR) and some less (e.g. CR-B). We also reordered the experiments according to their appearance in the text; same for the supplementary figures. The jumping between experiments and figures results from a manuscript structure which is based on certain physical topics. Therefore, it is inevitable to refer only to one experiment. The figure references are thought to help to orientate while jumping back and forth. The objectives of the experiments are commented above.

Density Trend

I don't think that this term describes the quantity properly. For instance, 'trend' typically indicates a change in time, which is not the case here. Please find a better descriptor. I would suggest 'Normalised Cumulative (Particle) Density'?

Authors: We appreciate this suggestion and changed "density trend (DT)" to "normalised cumulative particle density (NCPD)".

Detailed comments

l. 29. bracket missing

Authors: Added.

l. 29. '..achieved with substantial contributions from Eulerian numerical...'

Authors: Done as suggested.

l. 31-33. I don't understand why this remark is made, see l. 64-69.

Authors: Changed (see line 33).

l. 41. or around S/W Ireland.

Authors: Done as suggested.

l. 44. Baltic, subsequently those

Authors: Done as suggested.

l. 96. value horizontal eddy viscosity: please check value. It seems odd that it is negative, and to the power of 10?

Authors: Please, keep in mind that we talk about bi-harmonic mixing. For comparison, in O'Dea et al. (2017) the same viscosity was chosen.

l. 98. Drag coefficient: units?

Authors: The drag coefficient is non-dimensional, but the roughness length is not, which has been added together with the allowed drag coefficient range (line 107-108).

l. 99. output: and vertical velocity?

Authors: We made some analyses of the vertical velocities, but they did not revealed anything new and are thus not shown.

l. 105. spinup period: is this enough? The North Sea has a residence time of several years.

Authors: Please, see the below Fig. R1.4.

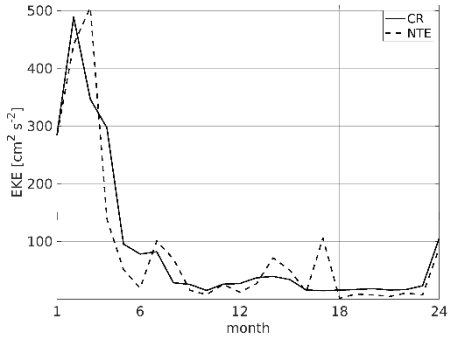

Fig. R1.4. Monthly EKE at 100 m averaged over the whole domain for 2014 and 2015.

l. 109-110. Really? Please check: I don't think hourly data are available.

Authors: It seems that for AMM7 hourly instantaneous data is no longer available on the Copernicus website (only daily means). Thanks for the hint. The text has been updated accordingly (line 121).

l. 112. operational FOAM-AMM7.

Authors: Done as suggested.

l. 155. The residual velocities and the velocity amplitudes... Please use the term 'residual velocities' throughout for this element (I will not indicate all occurrances).

Authors: Done as suggested.

l. 158. low residual velocities

Authors: Done as suggested.

l. 159. surely not only in the English Channel?

Authors: Extended (line 246).

l. 160. It is not clear to me how this is defined/quantified?

Authors: We found, as described in the text, that the model dynamics significantly change along this isobath.

l. 163. 'sea level oscillations': these are not presented: velocity oscillations?

Authors: "Sea level oscillations" is correct and relates to the previous sentence in the manuscript. SSH patterns were analysed but did not show new aspects and do not support the following analyses; thus they were discarded for the final set of figures.

l. 174. Why winter? How is 'winter' defined?

Authors: "winter" has been replaced by January and "summer" by July.

l. 177. The East Anglia plume is not defined by temperature, but by turbidity (and lies somewhat south of the location suggested here).

Authors: This is correct. The formulation was not appropriate and has been changed (line 268-271).

l. 178. Frisian front: is a summer feature separating temperature-stratified from wellmixed conditions.

Authors: The Frisian Front has been moved to July (line 274-276).

l. 182. 'a number of mesoscale features': it is not clear to me what is meant here.

Authors: This term relates to the patterns of the temperature gradients (Fig. 2f) in the deep ocean. They coincide with the patterns of velocity magnitudes (Fig. 2a) and have sizes of tens of kilometres.

l. 183. '...compare with...': it is not clear to me what should be compared.

Authors: Done as suggested.

l. 184. Fig S2a: why is this fig in the supplementary material?

Authors: For a clearer structure, the figures in the main manuscript only show January. To give an impression of the situation in July, too, we put all of these results on one page in the supplementary material.

l. 188. NTE: why does the narrative jump to this here? What about stratification?

Authors: The NTE is mentioned to proof the influence of tides. Stratification is also different in the NTE and CR, that is, the velocity field is also affected by stratification.

l. 189. 'much of what is known': please specify.

Authors: Done as suggested (line 280).

l. 192-205: please better specify/explain variables.

Authors: Done as suggested (line 297-298).

l. 206. Why 25 h average (I can guess, but not everyone might). On which day? Why this day? Why one day?

Authors: The explanation for using a 24.84 h-period (changed from 25 h) is added to the text (line 298-300). The day (15.01.2015) is given in the figure caption but is also added in the text.

l. 212. difference: which was subtacted from which?

Authors: The text reads “difference … between the CR and NTE”, i.e. CR minus NTE. To make it clear, the caption of Fig. 2 and the text (line 306) have been improved.

l. 213. ’despite’: replace by ’In addition to’

Authors: Done as suggested.

l. 212-214: what do positive/negative values mean?

Authors: Positive/negative values mean reduction/increase of deformation by tides.

l. 216. ’significant importance’: what does it do to them?

Authors: The presence of deformation indicates the possible contribution of shear to horizontal mixing, e.g. Sanderson and Okubo (1986 and 1987).

Sanderson, B. G., & Okubo, A. (1986). An analytical calculation of two-dimensional dispersion. *Journal of the Oceanographical Society of Japan*, *42*(2), 139–153. https://doi.org/10.1007/BF02109101

Sanderson, B. G., & Okubo, A. (1987). Comments on the “shear effect” and diffusion in the Lagrangian framework. *Journal of the Oceanographical Society of Japan*, *43*(3), 183–196. https://doi.org/10.1007/BF02109218

l. 217. this is not presented?

Authors: Not for January, because the difference is shown instead. For July it is shown (Fig. S2d).

l. 218. I don’t understand this sentence/reasoning.

Authors: The inner Bay of Biscay is mainly dominated by mesoscale dynamics, e.g. eddies. If the deformation difference plot (Fig. 2h) shows patterns with approximately the size of eddies, it can be concluded that they cause them.

l. 229. This is a conclusion. Also: how can you tell, as the experiments were not set up in the same way?

Authors: The intercomparison was done with the same setup (2-D online advection) and showed only very small differences (see previous answer). To prevent doubts about the similarity of online and offline simulations, a short explanation about the used setups is given in the text (line 152).

l. 236. ARIANE user manual: please provide reference.

Authors: The website has been added (line 158-159).

l. 237-239. Then how, exactly, does the horizontal particle diffusion work? Is the 7 km grid really sufficient to explicitly resolve all horizontal turbulent diffusion processes as eddies?

Authors: As already said, there is no consensus about adding extra lateral diffusion to particle tracking (van Sebille et al., 2018). Furthermore, our tests showed that extra diffusion will lead to slightly noisier NCPD fields but will not change the patterns substantially (this was tested in previous experiments; see also Fig. R1.1). Concerning what the model can resolve, we give examples from Stanev and Ricker (2020) where this issue is explained in detail (line 98-101).

Stanev, E. V., & Ricker, M. (2020). Interactions between barotropic tides and mesoscale processes in deep ocean and shelf regions. Accepted in *Ocean Dynamics*.

l. 245: stripe: strip. Along the shelf edge? A figure may help here.

Authors: We use “stripe” throughout the text both having the same meaning. Fig. 9 has been referenced (line 176-177).

l. 248. Why use a different model?

Authors: Backtracking is not possible online. This has been mentioned in the text (line 151).

l. 250. Why at a constant depth, i.e. different (?) from the forward experiments? How can you then compare? Why at 1 m, and not at the surface as in the other experiments?

Authors: The backtracking experiment is rather a complement of the forward experiments and is not thought to be compared in detail with the forward experiments. Despite that, in the online simulation, the seeding is also at 1 m.

l. 258. 6 months? Why?

Authors: This was done for Fig. 4. After 6 months the resulting patterns can be seen nicely and contributes an impression of particle accumulation/dispersal for longer time scales than one month.

l. 259. only january: why?

Authors: The focus of the paper is on monthly time scales. As an example January was chosen. Due to the importance of stratification in summer, July was chosen as a second example (see comment below) and put into the supplementary material. Furthermore, changes in tidal and wind forcing are applied on 01 January 2015. Impacts of the changes in forcing on the dynamics can only directly be seen during the transition period. Analyses of later months would rather describe the new steady state.

l. 260. NTE also July: why?

Authors: To show a representative summer pattern.

Table 2. Please complete with release time. Backtracking: 1 m, not surface.

Authors: The caption has been improved. Note the changed order of Table 1 and 2.

l. 305. Why 12 h? The tidal period is (roughly) 12.5 h, so the difference between start and end point of the depicted loops are not the residual (or net transport), but still contain a tidal contribution.

Authors: This is correct. Thus, a 12.42 h period was chosen to show a full M_2 cycle. Further, it is mentioned that the “The difference between the start and end positions on the circular loops gives an estimate of the net transport, …” (line 357-358).

l. 318. Refer to fig 4 after ’different’.

Authors: Done as suggested.

Figure 4. After introducing DT, it is not clear to me why the plots of particle positions were included? If it is to point out that DT is a better way to visualise, one simple comparison figure should suffice.

Authors: As correctly mentioned, the advantage of NCPD is the better way to visualise particle accumulation. Nevertheless, Fig. 4 also shows important details, especially the plots after 6 months. Particle positions also contribute to a better understanding of NCPD. This is mentioned in the paragraph starting at line 410.

l. 324. It is not clear to me what the authors aim to point out here?

Authors: Now, the sentence refers to Sect. 4.3, where this point is discussed in detail.

l. 331. breaking internal waves: the hydrostatic NEMO model cannot represent these.

Authors: “breaking” removed.

l. 333. I don’t see the causal relationship here?

Authors: There are several dynamic processes prevailing at the continental slope. Most of them induce a net transport which in turn affect the particle dynamics. The text has been improved (line 382).

l. 342. flown: been transported? They don’t have wings...

Authors: Done as suggested.

l. 355. ambiguous: what is meant with this? If you mean that the accumulation patterns have high spatial variability (or something like that), then say that? Please also change other occurrences?

Authors: Done as suggested.

l. 366. off-shore

Authors: Done as suggested.

l. 372. reduced: smaller than for surface particles

Authors: Done as suggested.

l. 382. I’m not sure what exactly you’re indicating here.

Authors: Extended (line 436-437).

l. 397. Irish Sea. Why mention this specifically: there are other places, too.

Authors: Yes, they are listed at the end of the paragraph and in the following ones.

l. 412. ’possibly indicating’: can you quantify the scales to make this a firm statement?

Authors: Done as suggested (line 464).

l. 418. the front: which front? Also I’m not sure if there is a front in winter?

Authors: The flanks of the warm water plume from the English Channel were meant. The text has been improved accordingly (line 470).

l. 421. suggests: how?

Authors: Extended (line 473-474).

l. 427. variability: of what?

Authors: Extended (line 478).

l. 429. FEW: FWE?

Authors: Changed.

l. 435. 'smoothing': please be consistent (with the abbreviation), and use 'filtering' throughout.

Authors: Done as suggested.

l. 440. 'that disappears': one can't see this in difference plots?

Authors: This is true and has been replaced (line 491).

l. 442. this contradicts the previous sentence.

Authors: We don't see a contradiction. Vast shelf areas are affected in terms of bottom particle accumulation but the most affected ones are in the northern shelf and Norwegian Trench/Skagerrak. The text has been modified to clarify that (line 493).

l. 445. Remove of substantiate.

Authors: These differences are important but can also be seen by the comparison of Fig. 6e and 6g and Fig. 6f and 6h, respectively. Thus, these figures have not been shown. The hint to compare the respective figures has been added (line 497).

l. 453. 'differences': please specify.

Authors: Explained (line 506).

l. 469. 'side of particle supply': what exactly do you mean?

Authors: An explanation was is given in the previous sentence but has been extended for clarification (line 522-524).

l. 470. 'the particle supply is hampered by the front': what exactly do you mean?

Authors: Sentence added (line 522-524).

l. 468-470. So backtracking experiments do not produce realistic results, as interactions with frontal dynamics are non-reversible?

Authors: For areas with strong fronts and areas downstream this is true. This point has been added to the text (line 524-525).

l. 483-487. Please demonstrate this by providing wind data.

Authors: Please see Fig. S1.

l. 491. How could this work? Most fronts are absent in January.

Authors: Thanks, this was wrong (sentence removed).

l. 512. I don't understand this sentence.

Authors: The sentence means, that a surface NCPD <1 (=particle dispersal) and a bottom NCPD >1 (=particle accumulation) should be related to an upward movement of water similar to positive and negative divergence.

l. 528. So what is causing the up/downwelling there, then?

Authors: This is explained in the following sentence (line 584).

l. 548. So what does this experiment add?

Authors: A sentence in the conclusions has been added (line 615-617).

l. 578. 'thalweg': This is German, please find English equivalent. Also occurs elsewere.

Authors: Although “Talweg” is the German word, “thalweg” is the English translation and is commonly used in this sense.

l. 587. ’floating marine debris’: only floating?

Authors: Actually it has to be “neutrally buoyant floating marine debris which is released at the sea surface and sea floor”. These characteristics should be clear from the manuscript and thus it is abbreviated as “floating marine debris”.

l. 589 etc.: Please provide links/references to data sources.

Authors: The links and references for data and models have been shifted from the text to this section.

Figure captions: please put graph labels before the descriptors, not after.

Authors: Done as suggested.

Figure 3, caption: what are the isobaths in a) and b)?

Authors: The black isobath (200 m) is mentioned in Fig. 1 and is the same in all figures. For Fig. 3c and d the isobaths are mentioned in the caption of Fig. 3.

Figure 5, 7 caption: southern bight, not German Bight, please check throughout.

Authors: Thanks for the hint. Done as suggested.

Figure 5: ’annual mean’ is depicted, not ’monthly average’?

Authors: Yes, changed accordingly.

Figure 7: distance: along transect?

Authors: Yes, for clarity, a sentence has been added in the caption.

Figure 8, caption: I’m not sure what’s meant with the last sentence.

Authors: It is the caption for (b) (=CR-B results). Should be clear after changing the position of the graph levels.

Figure 9. It is not clear to me why a portion of the particles is purple? Surely they have all potentially changed depth?

Authors: All particles of this experiment are purple. Purple was chosen to differentiate them from colours appearing in the colour bar. In each plot, the purple dots show the particles used to calculate the depth change of the respective figure (blue-red-coloured grids). The depth change is shown at the initial particle positions.

Reply to:

Interactive comment on "Circulation of the European Northwest Shelf: A Lagrangian perspective" by Marcel Ricker and Emil V. Stanev

Anonymous Referee #2

Received and published: 24 January 2020

We thank reviewer #2 for the constructive review of our paper. We provide point-by-point answers in the attached pdf.

Summary

The authors have performed a set of Lagrangian particle tracking experiments to study the water circulation on the European Northwest Shelf (ENWS). Several scenarios were simulated, with particles (passive tracers, or water masses) released at surface and seafloor, and simulated forwards for up to 1 year, plus one case with backwards simulations. A property called "density trend" is defined to aid the analysis of the spatial accumulation of particles.

General comments

As the authors themselves point out, several modeling studies have looked at the ENWS, but not so many studies have applied Lagrangian methods, at least not for the whole area. The simulated scenarios are sensible, and the discussion contains several interesting comments and findings, though nothing groundbreaking. The main weakness of the paper is that the discussion would need a more clear structure, and be better linked to well defined motivation/objectives. But after improving the structure (i.e. major revision) and some details as discussed below, I would find this manuscript suitable for publication.

Authors: Thank you. We improved the structure (see also a comment below) of the paper and clarified the objectives of the respective experiments (line 188-196). The minor comments have been implemented as given below. Note that the quantity "density trend (DT)" has been renamed to "normalised cumulative particle density (NCPD)".

Specific comments

Line 29: Missing end parenthesis.

Authors: Added.

Lines 40-50 discusses typical current patterns. It would be helpful with a figure with arrows to better follow this description.

Authors: We added schematically grey arrows in Fig. 1 to indicate the general shelf sea circulation (line 42-43). To complement this, we added “Howarth (2001)” (line 52-53) as a reference for North Sea circulation.

Line 50: Could ref to Fig2c for the comment about low salinity along coast.

Authors: To improve the structure, we want to prevent mixing up the order of the figures appearances. However, Fig. 2d is mentioned in Sect. 2.3 with respect to the low salinity along the coasts.

Lines 50-52: This major hypothesis should be reflected also in abstract.

Authors: Done as suggested (line 24).

Lines 60-62: Sentence is a bit hard to read.

Authors: Improved (line 65).

Line 75: Should mention here that vertical mixing is also not considered. This is an important point, that should also be discussed/justified.

Authors: We made clear in the revised manuscript that the used Lagrangian techniques aim at giving a new view on velocity field in the North Sea. In other words, the paper is about velocity, not so much about turbulence. We do not analyse the propagation and mixing of particles. In our setup, particles released in NEMO are always advected in 3-D by (u,v,w). That is, the particles are neutrally buoyant (added in line 163-164) and can be interpreted as following the pathways of water parcels (Blanke and Raynaud, 1997). Because we study the properties of the velocity field, additional horizontal and vertical turbulent mixing is not introduced for particle tracking. As a consequence, the presented analyses are analyses of velocity properties and not of the effects of mixing (added in line 83-84 and 163-164).

Nevertheless, in terms of T/S, the water column is well mixed in January, thus the model physics can be treated as correct. The specific properties of the velocity field explains the difference of NCPD at the surface and bottom.

Implementations of turbulent mixing in Lagrangian tracking is mostly done by random walk schemes. The effect of horizontal diffusion is shown in Fig. R.2.1. We want to emphasise that the implementation of horizontal (van Sebille et al., 2018) and, in particular, vertical diffusion (van Sebille et al., 2020) in particle tracking are ongoing scientific subjects.

van Sebille, E., Aliani, S., Law, K. L., Maximenko, N., Alsina, J., Bagaev, A., et al. (2020). The physical oceanography of the transport of floating marine debris. Environmental Research Letters. https://doi.org/10.1088/1748-9326/ab6d7d

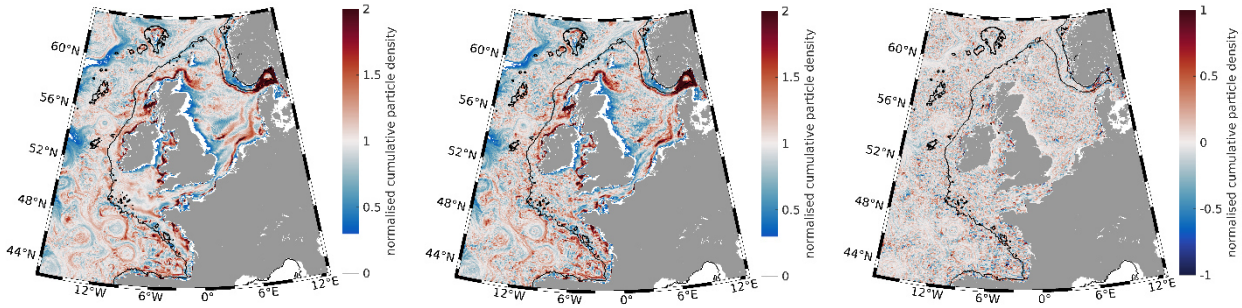

Fig. R2.1. Surface January 2015 NCPD without (left) and with (middle) additional horizontal diffusion in particle advection obtained from offline simulations. The right panel shows the difference without minus with diffusion.

Line 89: It is not clear whether the area of Fig 1 is identical to the AMM7 area, or if this is a subset?

Authors: It is a subset and has been added to the text (line 116-117).

Line 90: AMM7 is called a model, but perhaps “model setup” is more precise?

Authors: Done as suggested (line 95).

Line 93: Here the term “tracer” is used. It should be made clear whether tracer and particles are the same thing in this study.

Authors: Thanks for the hint. The use of “tracer” and “particle” should not be mixed up. Thus, Lagrangian particles have been defined (line 81-82) as well as the model tracers (T and S; line 102).

Line 95: Please provide a reference or justification for the choice of eddy diffusivity. It should be commented that this is constant throughout the area (which is not true in reality).

Authors: Please see, e.g. O’Dea et al. 2012 for a comparable setup of NEMO. The constant value of eddy diffusivity has been mentioned in line 104.

Line 96: Eddy viscosity should be a positive number.

Authors: Please keep in mind that we use biharmonic, not Laplacian mixing.

Section 2.2: More information should be given about the drifter type/characteristics/name, as near-surface drifters are affected by a varying degree of Stokes drift and wind drag, see e.g. Röhrs, J., K. H. Christensen, L. R. Hole, G. Broström, M. Drivdal, and S. Sundby (2012), Observation-based evaluation of surface wave effects on currents and trajectory forecasts, Ocean Dyn., 62, 1519–1533

Thus, a missing contribution from Stokes drift can possibly explain why the model currents are too slow in the comparison. Alternatively, SVP drifters (15m depth) from the Global Drifter Program could be used to validate the model current, so that Stokes drift would not be an

issue. Also a plot of the complete drifter trajectories should be shown, to justify whether they cover a substantial part of the area, or just locally to their deployment location.

Authors: In this paper the focus is on analysing Lagrangian trajectories (no real drifters). As far as Stokes drift is concerned, please see our earlier publication (Röhrs et al. (2012) and Stanev et al. (2019) are now cited in line 324-325) as well as the one discussing technical details about real drifters by Callies et al. (2017) (line 132). The restriction to the German Bight is given in line 136.

Callies, U., Groll, N., Horstmann, J., Kapitza, H., Klein, H., Maßmann, S., & Schwichtenberg, F. (2017). Surface drifters in the German Bight: model validation considering windage and Stokes drift. *Ocean Science*, *13*(5), 799–827. https://doi.org/10.5194/os-13-799-2017

Line 148/Table1: The number of comparison points should be provided.

Authors: Added in the Table. Note the changed order of the Tables.

Section 2.3. This discussion is a bit messy, and does also belong in the results section, rather than under “material and methods”.

Authors: All results of Sect. 2.2 and 2.3 have been shifted to the results (note the rearranged order of the manuscript).

Line 184: It could be made clear (the first time) that Figure S2a refers to figure 2a in the supplements.

Authors: Done as suggested (line 252-253).

Line 207: could be commented that the Molinari and Kirway study is for the Caribbean during summer, thus quite different conditions.

Authors: This is correct and has been added (line 301).

Line 240: It should be commented (and discussed) that vertical mixing is not included.

Authors: The neglection of vertical mixing and how the movement of particles can be interpreted is added to the text.

Line 242: Should also be mentioned here that particles are released over the whole domain.

Authors: Done as suggested.

Line 244-246: The seeding locations of CR-V should also be shown on a figure

Authors: Showing the initial positions horizontally would require an own figure. Due to the amount of figures we decided to not add another one but to show these positions exemplarily for the lowest depth layer in Fig. 9e. We also improved the text accordingly (line 175-177).

Line 248: It should be mentioned explicitly that a separate offline trajectory model has to be used for the backwards simulations, as this is not possible to do with online simulations. However, a forward simulation with this offline model should also be done to benchmark it against the online forward simulations.

Authors: Such comparison has been made during the preparation of the manuscript and is mentioned in the text in line 151-153. The comparison in terms of NCPD using the results from

an online run without vertical advection and the same setup in OpenDrift for January 2015 is shown in Fig. R2.2 (NCPD online minus offline). The differences are rather minor. In text, the necessity of an offline model has been added (line 151).

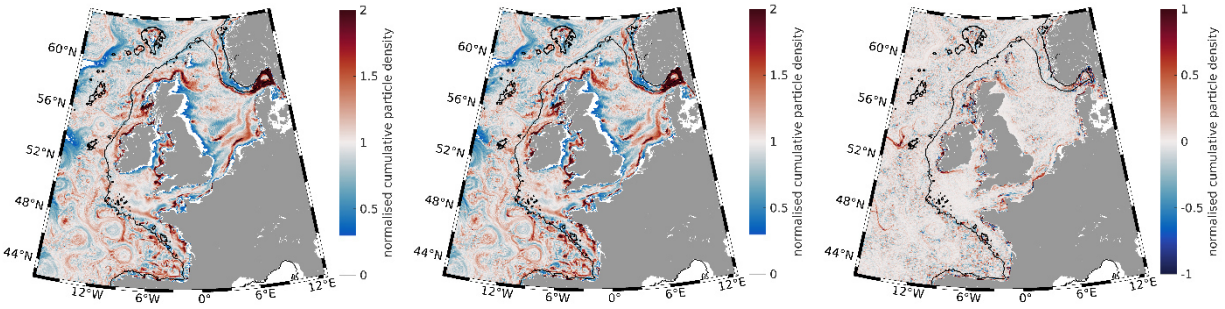

Fig. R2.2. Surface January 2015 NCPD online 2-D (left), offline (middle) and the difference online minus offline (right).

Lines 274-279: What would be the difference between “density trend” and “residence time”?

Authors: Residence time (RT) is defined as $\bar{t}_{\mathrm{w}} = \mathrm{V}_{\mathrm{S}}^{0}/\bar{J}_{\mathrm{V}}^{0}$ where $\mathrm{V}_{\mathrm{S}}^{0}$ is the total volume in the ocean reservoir and $\bar{J}_{\mathrm{V}}^{0}$ is the mean flux through the reservoir in unit time in case of a steady state (superscripted 0); see, e.g. Whitfield (1979). It measures the time needed to completely replace the volume of water in a certain oceanic region. If the RT is referred to an individual water element Y, the RT formula can be rewritten as $\bar{t}_{\mathrm{Y}} = \mathbf{Y}_{\mathrm{S}}^{0}/\bar{J}_{\mathrm{Y}}^{0}$, where $\mathbf{Y}_{\mathrm{S}}^{0}$ is the total mass of Y and $\bar{J}_{\mathrm{Y}}^{0}$ is its flux through the reservoir. In our study, Y can be interpreted as a particle. Then, NCPD would be the ratio of $\bar{J}_{\mathrm{Y}}^{0}$ and $\bar{J}_{\mathrm{Y,U=0}}^{0}$ with (u,v,w) = 0, because they are the sum of particles over a certain period of time. Although both fluxes have the unit [mass/time], the latter flux could be interpreted as $\mathbf{Y}_{\mathrm{S}}^{0}$, because it is constant in time. With this interpretation, NCPD is $1/\bar{t}_{\mathrm{Y}}$ with the unit [1/month]. That is, NCPD is proportional to the inverse RT (line 227-228).

Whitfield, M. (1979). The mean oceanic residence time (MORT) concept - a rationalisation. *Marine Chemistry*, *8*(2), 101–123. https://doi.org/10.1016/0304-4203(79)90010-0

Line 278: “motionless situation” is a bit unclear, please rewrite sentence.

Authors: Done as suggested (line 215-217).

Line 302-304: Please clarify what is meant here.

Authors: Done (line 352-353).

Line 461: extra space after “Channel”

Authors: Removed.

Section 3 is a bit lengthy, and hard to read due to jumping back and forth between the experiments and referring to many figures. Making it a bit more compact and structured would help.

Authors: We tried to split the sections into equally long sections as well as in a Eulerian and a Lagrangian results part. We also reordered the experiments according to their appearance in the text; same for the supplementary figures. The jumping between experiments and figures results from a manuscript structure which is based on certain physical topics. Therefore, it is inevitable to refer only to one experiment. The figure references are thought to help to orientate while jumping back and forth. We still find them helpful and decided to keep them.

Figures

There are a lot of composite figures/maps of the area of interest. These are quite small and hard to read when printed on A4 paper. Could whitespace be reduced somehow?

Authors: We reduced the white space as much as possible, especially in Fig. 2. Insets have been enlarged. All labels should be readable now.

In the figure captions, the letters a), b)... should rather be placed before the explanation, and not after

Authors: Done as suggested.

Figure 2: CR and NTE should be written explicitly as “control run” and “no tides experiment”, so that the figure can be read and understood also before reading the main text. Same for other figures.

Authors: Good idea. Done as suggested. Same for NCPD.

Line 847: und -> and

Authors: Changed.

Figure 3: a bit much spaghetti here, perhaps use even fewer than every 5th trajectory?

Authors: We changed it to every 8th particle. For us, the present figure is a good compromise between visualising the currents for both the surface and bottom as well as covering most of the domain with trajectories. We also remark, that we will provide this figure in high quality to OS, so that the reader can zoom in and see specific details.

Figure 4: Caption is quite hard to read. The ‘+’ and ‘-’ symbols are presumably placed “by hand”? This is generally ok, but they are quite many, and sometimes slightly displaced, perhaps to avoid overlap? So in practice I don’t think these symbols work very well here. Could the point be visualized by another, more objective measure?

Authors: For Fig. 4, NCPD can be interpreted as a quantitative measure for particle accumulation. Thus, we decided to avoid any of these markers and we emphasise, that we describe examples of pronounced features (line 373-375 and 565).

Figure 5: Title of lower figure is “monthly average”, but I guess it should be “yearly average”, or “average of months”

Authors: This is correct and has been changed accordingly.

References

Please update this reference, where you refer to a discussion paper: Dagestad, K.- F., Röhrs, J., Breivik, Ø., and Ådlandsvik, B.: OpenDrift v1.0: a generic framework for trajectory modelling, Geosci. Model Dev., 11, 1405–1420, https://doi.org/10.5194/gmd-11-1405-2018, 2018.

Authors: Done as suggested.

Circulation of the European Northwest Shelf: A Lagrangian perspective

Marcel Ricker[1,2*] and Emil V. Stanev[2]

[1]University of Oldenburg, Institute for Chemistry and Biology of the Marine Environment, Carl-von-Ossietzky-Straße 9-11, 26111 Oldenburg, Germany

[2]Institute of Coastal Research, Helmholtz-Zentrum Geesthacht, Max-Planck-Straße 1, 21502 Geesthacht, Germany

*Corresponding author: E-mail: marcel.ricker@uni-oldenburg.de

Abstract

The dynamics of the European Northwest Shelf (ENWS), the surrounding deep ocean, and the continental slope between them are analysed in a framework of numerical simulations using Lagrangian methods. Several sensitivity experiments are carried out in which (1) the tides are switched off, (2) the wind forcing is low-pass filtered, and (3) the wind forcing is switched off. To measure particle accumulation, a quantity named the "normalised cumulative particle density (NCPD)" is introduced. Yearly averages of monthly results in the deep ocean show no permanent particle accumulation areas at the surface. On the shelf, elongated accumulation patterns persist on yearly averages, often occurring along the thermohaline fronts. In contrast, monthly accumulation patterns are highly variable in both regimes. Tides substantially affect the particle dynamics on the shelf and thus the positions of fronts. The contribution of wind variability to particle accumulation in specific regions is comparable to that of tides. The role of vertical movements in the dynamics of Lagrangian particles is quantified for both the eddy-dominated deep ocean and for the shallow shelf. In the latter area, winds normal to coasts result in upwelling and downwelling illustrating the importance of vertical dynamics in shelf seas. Clear patterns characterising the accumulation of Lagrangian particles are associated with the vertical circulations.

1 Introduction

The European Northwest Shelf (ENWS) (Fig. 1) is among the most studied ocean areas worldwide. Numerous reviews have presented details of its physical oceanography (e.g. Otto et al., 1990; Huthnance, 1991). Understanding the dynamics of the ENWS has been achieved with substantial contribution from Eulerian numerical modelling (Maier-Reimer, 1977; Backhaus, 1979; Heaps, 1980; Davies et al., 1985; Holt and James, 1999; Pohlmann, 2006; Zhang et al., 2016; Pätsch et al., 2017). In contrast, the usefulness of Lagrangian methods for a comprehensive understanding of the ENWS dynamics has not been widely investigated heretofore.

In the following, we briefly summarize some basic oceanographic knowledge about the ENWS (the study area is shown in Fig. 1). The slope current dynamics and exchanges between the deep ocean and shelf have been analysed by Huthnance (1995), Davies and Xing (2001), Huthnance et al. (2009) and Marsh et al. (2017); Lagrangian drifter experiments in this area have been described by, e.g. Booth (1988) and Porter et al. (2016). The prevailing westerlies induce on-shelf water transport from the Celtic Sea up to the Outer Hebrides (Huthnance et al., 2009). Water entering the Celtic Sea flows either into the English Channel, into the Irish Sea via St. George's Channel or around southwest Ireland (grey arrows in Fig. 1 schematically show the principal shelf circulation). The water exiting the Irish Sea flows around the Outer Hebrides and joins the on-shelf transported water. Part of this water enters the North Sea, mainly via the Fair Isle Current, where it begins an anti-clockwise journey through the North Sea. The third path of waters entering the North Sea originates from the Baltic Sea, subsequently those waters are integrated into a complex system of currents in the Skagerrak and the Norwegian Trench. In this area, the Atlantic and Baltic Sea waters undergo strong mixing. Along the southern slope of the Norwegian Trench, a branch of the European Slope Current flows toward the Baltic Sea, while a current flowing in the opposite direction follows the northern slope of the trench. In addition, large river runoff influences the water masses in the North Sea and along the Scandinavian coast, explaining the low salinity along coastal areas. Further details of the North Sea circulation can be found in, e.g. Howarth (2001) and in the above-mentioned reviews. The major hypothesis in the present study is that although

54 the North Sea is very shallow, it contains an important vertical circulation. Revealing such
55 characteristics is the first objective of the present study.
56
57 Much is known about the thermohaline fronts on the ENWS and its estuaries (Simpson and Hunter,
58 1974; Hill et al., 2008; Holt and Umlauf, 2008; Pietrzak et al., 2011). Although large parts of this ocean
59 area are vertically well mixed, seasonal and shorter-term variability lead to pronounced differences in
60 the positions and strengths of the fronts; freshwater fluxes are also important, particularly in shallow
61 coastal areas. Krause et al. (1986), Le Fèvre (1986), Belkin et al. (2009), Lohmann and Belkin (2014),
62 Mahadevan (2016) and McWilliams (2016) addressed the biological consequences of frontal systems,
63 and the frontal physics are summarized in Simpson and Sharples (2012). However, to the best of the
64 authors' knowledge, the frontal dynamics of the ENWS have not been addressed from a Lagrangian
65 perspective; therefore this will be the second objective of our study.
66
67 Most previous studies that employed Lagrangian particle tracking in the region of the ENWS
68 (Backhaus, 1985; Hainbucher et al., 1987; Schönfeld, 1995; Rolinski, 1999; Daewel et al., 2008; Callies
69 et al., 2011; Neumann et al., 2014 and Marsh et al., 2017) addressed only part of the region studied
70 herein. Hence, our third objective is to provide a comparison among the specific hydrodynamic regimes
71 in different areas of the ENWS and exchanges between these areas. One example has been recently
72 provided by Marsh et al. (2017) for part of the European Slope Current. Lagrangian approaches applied
73 to other ocean regions can be found in, e.g. Bower et al. (2009) for the North Atlantic, Paparella et al.
74 (1997) for the Antarctic Circumpolar Current, Reisser et al. (2013) for Australia, van Sebille et al.
75 (2015) for the world ocean, Maximenko et al. (2018) for tsunamis, Froyland et al. (2014) and van der
76 Molen et al. (2018) in terms of connectivity studies.
77
78 The present study was initiated in the framework of a project studying the fate of marine litter in
79 the North Sea (Gutow et al, 2018; Stanev et al, 2019). Here, we extend the area of our analyses to
80 include the entire ENWS, the European Slope Current, the Bay of Biscay and parts of the Northeast
81 Atlantic. Unlike our recent studies, herein, we address virtual Lagrangian particles ("particles" in the

following) and not real drifters. These particles are transported only by 3-D ocean currents (turbulence, Stokes drift and wind drag are not considered). Thus, this study aims at giving a Lagrangian representation of velocity field of the ENWS and the surrounding deep ocean.

In Sect. 2, we will describe the model, its setup and the Lagrangian experiments. In Sect. 3.1 and 3.2, Eulerian model results and model validations are presented followed by Lagrangian model results and sensitivity experiments being discussed in Sect. 4.1 to 4.5. The paper ends with a brief conclusion in Sect. 5.

2 Materials and methods

2.1 The numerical model

The Nucleus for European Modelling of the Ocean (NEMO) hydrodynamic ocean model is used in this paper (Madec, 2008). For this study, the Atlantic Margin Model configuration with a 7 km resolution (AMM7; Fig. 1) of NEMO is chosen because it appears to be one of the best validated model setups for the ENWS (O'Dea et al., 2012 and 2017). The numerical model solves the primitive equations using hydrostatic and Boussinesq approximations. The horizontal resolution is $^1/_9°$ in the zonal direction and $^1/_{15}°$ in the meridional direction; that is, the resolution is approximately 7.4 km. This lateral resolution allows for resolving, e.g. tidal mixing fronts, modification of tidal ellipses by stratification, strong shear stresses induced by tides and eddies with diameter larger than 30-40 km. Not fully resolved are, e.g. frontal jets and shelf break downwelling (Stanev and Ricker, 2020). There are 297 × 375 grid points altogether and 51 vertical σ-layers. For tracer, i.e. temperature and salinity, advection, we employ the total variation diminishing (TVD) scheme, diffusion takes place on geopotential levels with a Laplacian operator (the constant horizontal eddy diffusivity is specified as 50 $m^2\ s^{-1}$). For momentum diffusion, a bi-Laplacian scheme is applied to act on the model levels (constant coefficient of = $-1\cdot10^{10}\ m^4\ s^{-1}$). The generic length scale (GLS) k-ε scheme is used as the turbulence closure scheme; the bottom friction is nonlinear with a log-layer structure, a roughness length of $3\cdot10^{-3}$ m and a drag coefficient range of $1\cdot10^{-3}$ to $3\cdot10^{-3}$. The baroclinic time step is 300 s. The output, including the salinity (S), temperature (T), velocities (u, v) and sea surface height (SSH), is written hourly.

The atmospheric forcing is provided by the UK Met Office atmospheric model with a 3-h temporal resolution for the fluxes and an hourly resolution for the 10 m wind and air pressure. The model uses climatological river runoff, and tidal forcing is prescribed at the open boundary. The period of integration considered here spans from 01 January 2014 to 31 December 2015 of which the first year is the spin-up period. The analyses of the results are performed for the area between 42.57° N–63.50° N and 17.59° W–13.00° E, which is slightly smaller than the model domain to avoid effects due to the open boundaries.

Although part of this study could be performed using the freely available Forecasting Ocean Assimilation Model (FOAM) AMM7 data (marine.copernicus.eu), we run the abovementioned model to (1) perform Lagrangian simulations online , (2) taking into account time scales shorter than days and (3) carry out some additional sensitivity experiments. In contrast to the operational FOAM AMM7 model, the data are not assimilated here. In the following, the basic experiment is referred to as the control run (CR). In one sensitivity experiment, the tides are turned off; this experiment is referred to hereafter as the nontidal experiment (NTE). In two other sensitivity experiments, the wind forcing is low-pass filtered with a moving time window of one week (referred to as the filtered-wind experiment, FWE) or completely turned off (the nonwind experiment, NWE). The changes in the model forcing are applied on 01 January 2015.

2.2. Validation data

For validation of SST, data from the Operational Sea Surface Temperature and Ice Analysis (OSTIA) system is used, which provides a gap-free synthesis of several satellite products (Donlon et al., 2012). Velocities have also been validated using 9 passive GPS surface drifters; these drifters provide the most appropriate type of in situ data for validating the model's ability of particle advection. The drifters, which have a bottom-mounted sail to reduce direct wind drag, were designed to be moved by the upper 1 m of the ocean (see Callies et al. (2017) for a technical description of the drifters). The drifters were released in the German Bight during RV *Heincke* cruise HE445, and their position was sent every ~20

minutes from May to July 2015. The dataset is freely available (Carrasco and Horstmann, 2015) and to the best of the authors' knowledge, it is the only GPS drifter dataset available for the ENWS during the period of the simulations analysed herein. For validation, the model velocities are interpolated to the drifter positions in space and time. Drifter velocities are also compared with independent observations using HF radar data. The HF radar system described by Stanev et al. (2015) and Baschek et al. (2017) consists of 3 measurement stations covering most of the German Bight and measures ocean surface velocities.

2.3 Particle release experiments

Particles are released in the hydrodynamic model, and their propagation is used to analyse the transport properties. The experiments were carried out "online"; that is, the particle trajectories were computed within the hydrodynamic model at every time step. Additional experiments were carried out "offline" using the model velocity output. High-frequency processes and vertical transport are better accounted for in the former experiments, whereas backtracking is only possible offline. An intercomparison between the online and offline integrations using the same particle setup demonstrated that neither approach leads to drastic differences when comparing 2-D particle transport properties.

The online advection of particles was achieved by the freely available open-source ARIANE model. The version of ARIANE implemented in NEMO has frequently been used in other studies, e.g. Blanke and Raynaud (1997) and Blanke et al. (1999). Further details of the ARIANE model can be found in the appendix of Blanke and Raynaud (1997) and in the ARIANE user manual (stockage.univ-brest.fr/~grima/Ariane/). Beaching is not possible; that is, the total number of particles remains constant over time. An extra wind drag is not used, nor is additional horizontal and vertical diffusion for the particles (pure Lagrangian particles). Actually, velocity gradients together with a small advection time step (van Sebille et al., 2018) provide a sufficiently high shear diffusion. The vertical velocity is taken into account and the particle positions are written hourly. Particles are neutrally buoyant and provide a Lagrangian representation of the velocity field.

Different seeding strategies were implemented. In one class of experiments (#1–4 in Table 1), the particles were seeded laterally at 1 m (surface particles), as well as in the grid cells just above the seafloor (bottom particles) over the whole domain. In the second experiment (#5 in Table 1) named CR-B, the particle tracking process was carried out offline. For this purpose, the freely available open-source model OpenDrift (Dagestad et al., 2017) was used, in which the particles were advected by a 2nd-order Runge–Kutta scheme. The offline calculation was performed backward in time at a constant depth with a velocity input time step, a model time step and an output time step of 1 h. The particle release depth in this experiment was 1 m. In a third experiment (#6 in Table 1) named CR-V, particles were released in a 100 km wide stripe extending oceanward from the 150 m isobath starting in the Bay of Biscay and ending north of the Shetland Islands at 61.7° N (red and blue coloured area in Fig. 9a–d). In this experiment, particles were seeded vertically every 20 m; this is exemplarily shown for the depth 900–1,000 in Fig. 9e.

The seeding strategy was consistently executed as follows. The initial distribution of particles was uniform with 1 particle per model grid cell, that is, 64,831 particles per depth layer for the whole domain (experiments #1–5 in Table 1) and a total of 345,011 particles in experiment #6. In the CR and CR-V (experiments #1 and 6, respectively), particle release was repeated on the first day of every month in 2015, and particles were traced for 1 month. Thus, 12 data sets, each including 1 month of trajectory data, were generated. Additionally, for the seeding in January, the particle positions were saved for 6 months. The FWE, NWE and CR-B (experiments #3–5, respectively) were conducted only for January 2015 whereas the NTE (experiment #2) was run until the end of July 2015.

Experiment #1 aims to understand and visualise the general circulation of the ENWS at both the surface and bottom. The uniform initial distribution of particles enables a comprehensive Lagrangian representation of surface and bottom dynamics over the whole domain. This experiment will also be used to analyse accumulation and dispersal areas as well as vertical dynamics and frontal effects. Further, it serves as the reference run for the sensitivity experiments. The sensitivity experiments (experiments #2–4) are performed to assess the influence on Lagrangian dynamics of some of the most

194 important drivers for particle advection, i.e. tides and wind. Experiment #5 supports the analyses of
195 vertical shelf dynamics and complements experiment #1. Experiment #6 provides a 3-D particle seeding
196 along the continental slope to study the dynamics there.
197
198 **Table 1**: Summary of the particle release experiments; further details are given in Sect. 2.3. Surface
199 release is done at 1 m depth and bottom release one grid cell above the sea floor. Particle release was
200 done once at the beginning of each month.

# (abbr.)	Particle advection		Spatial seeding			Integration time	Details
	Online	Offline	Whole domain	Shelf edge	Vertical		
1 (CR)	x		x		surface & bottom	12 x 1 month	3-D particle motion
2 (NTE)	x		x		surface & bottom	January + July	no tides,3-D
3 (FWE)	x		x		surface & bottom	January	filtered wind, 3-D
4 (NWE)	x		x		surface & bottom	January	no wind, 3-D
5 (CR-B)		x	x		surface	January	backtracking, 2-D
6 (CR-V)	x			x	every 20 m	12 x 1 month	only shelf edge, 3-D

201
202 *2.4 Normalised cumulative particle density*
203 The analyses of the results will focus on typical Lagrangian properties, e.g. the positions of the particles
204 and their trajectories. Such a presentation could be considered inferior compared with the Eulerian
205 presentation, which displays the concentrations of properties. However, from these Lagrangian
206 characteristics, one can derive properties similar to the concentration that can represent the
207 "compaction" process of particles in certain areas or identify the areas that are more frequently visited
208 by the particles. These properties related to particle density allow the areas in which particles
209 accumulate to be identified.
210
211 Different approaches to quantify particle accumulation have been proposed (Koszalka and LaCasce;
212 2010; Koszalka et al., 2011; van Sebille et al., 2012; Huntley et al., 2015). Below, in addition to the
213 typical Lagrangian properties, a property named the "normalised cumulative particle density (NCPD)"
214 is introduced that measures the number of particles that have visited each grid cell during a certain time
215 interval. This quantity is normalised by the corresponding number of initial particles in the respective

NCPD grid cell for the same time interval (in our case 1 particle per grid cell), which corresponds to a motionless situation:

$$NCPD(x, y, t_n) = \frac{\sum_{i=0}^{n} N_{u\neq 0}(X,Y,t_i)}{\sum_{i=0}^{n} N_{u=0}(X,Y,t_i)} \quad (1)$$

where *NCPD* is the normalised cumulative particle density, (*X*, *Y*) are the coordinates of an arbitrary grid cell in longitudinal and latitudinal direction, respectively, with dimensions (*dX*, *dY*), *n* is the number of time steps from t_0 to t_n, *u* is the velocity field and *N* is the number of particles at time step *i* in grid (*X*, *Y*). In the present study, (*dX*, *dY*) represent the model grid dimensions (*dx*, *dy*), but could be larger or smaller for other applications. A NCPD greater (smaller) than unity corresponds to more (fewer) particles, which are identified in a grid cell on average, than there would be without currents. Thus, the NCPD can be interpreted as the percentage of the initial number of particles averaged over time, or as proportional to the inverse residence time.

The definition of the NCPD is not straightforward if the initial particle concentration is zero in some areas. If the number of particles in some areas remains small (e.g. areas close to an inflow-dominated open boundary or divergence zones), the statistical confidence of this property cannot be ensured. Therefore, areas where the NCPD is less than 30 % are excluded from the analysis (white areas in the following figures). In the present study, the focus will be on monthly time scales (t_n = 1 month). Choices of (*dX*, *dY*) and of the particle seeding have been made accordingly. For comparison, for integration times longer than one month, large areas remain free of particles; integration times shorter than one month would cause rather noisy results.

3 Eulerian model results

3.1 Analysis of the simulated dynamics

The circulation of the CR is very diverse in different model areas, but the differences among the dynamic regimes in the CR are most pronounced between the deep ocean and the shelf. The residual

243 velocities (U) and velocity amplitudes for January 2015 (Fig. 2a and 2b) show basically two regimes:
244 an eddy-dominated regime west of the continental slope and a tidally dominated regime on the shelf.
245 The latter is characterized by relatively low residual velocities (Fig. 2a) and large velocity oscillations
246 in the English Channel, Southern Bight, Irish Sea and Celtic Sea (Fig. 2b). The transition between these
247 two regimes occurs along the 200 m isobath (Fig. 2a), which can be considered a separation line between
248 the dynamics of the shelf and deep ocean. A sequence of mesoscale eddies is developed offshore of the
249 western shelf edge with a dominant one in the Rockall Trough (Fig. 2a and 2b), which are also readily
250 visible in the corresponding SSH pattern (not shown). The largest amplitudes of the sea level
251 oscillations are observed around the British Isles and along the southern coasts of the German Bight.
252 The dominant wind direction is from the west due to the prevailing westerlies (Fig. S1 in the
253 supplementary material).
254
255 The simulated thermohaline characteristics are consistent with the existing knowledge: the coastal
256 waters, particularly those in the German Bight, are less saline (Fig. 2c) and represent typical regions of
257 freshwater influence (ROFIs). In the German Bight, most of the low-salinity water originates from the
258 Rhine, Ems, Weser and Elbe Rivers and spreads along the Dutch, German and Danish coasts before it
259 reaches the Skagerrak, where it mixes with the low-salinity outflow from the Baltic Sea. The pattern of
260 the salinity gradient (Fig. 2d) reveals features along the coasts and at the major fronts in the German
261 Bight. Additionally, the two current branches in the Norwegian Trench associated with two opposing
262 flows (one flowing to the east along the southern slope and another flowing in the opposite direction
263 along the northern coast) are also easily observed as areas characterised by large salinity gradients.
264
265 In January, the overall temperature distribution is characterized by cold temperatures on the shallow
266 shelf and a south-north temperature gradient in the deep water south of Ireland (Fig. 2e). A warm water
267 plume exits the English Channel (Fig. 2e) and traces the pathway of warm Atlantic water in the North
268 Sea, which is also known from the satellite observations of Pietrzak et al. (2011). At the northern
269 boundary of this plume, the East Anglia Plume is known to transport suspended particulate matter
270 (SPM) to the northeast. Along with a second plume extending into the Irish Sea, they are visible as

strong temperature gradients (Fig. 2f). The temperature gradient also reveals a number of mesoscale features occurring in the deep ocean along the rims of currents (compare Fig. 2f with 2a). In July, the warmest temperatures can be found in the Bay of Biscay and along the coasts of the shallow shelf, especially on the Armorican Shelf (Fig. S2a). The July temperature distribution is also characterized by well-pronounced temperature gradients, e.g. the Frisian Front located somewhat north of the Dutch coast. The simulated gradients along the Celtic Sea Front, Ushant Front, Islay–Malin Head Front and the Flamborough Head Front (black circles in Fig. S2a) support the results of Pingree and Griffiths (1978). The disappearance of these fronts in the results of the NTE demonstrates that they are tidal mixing fronts (see Fig. S2a and S2b). Overall, Fig. 2 supports much of what is known from previous studies about the general dynamics and thermohaline characteristics of the ENWS (e.g. Pätsch et al., 2017).

Understanding the differential properties of currents is of utmost importance to understand the propagation of Lagrangian particles. Therefore, we will present a brief analysis of deformation, as proposed by Smagorinsky (1963):

$$|D| = \sqrt{{D_T}^2 + {D_S}^2} = \sqrt{\left(\frac{\partial u}{\partial x} - \frac{\partial v}{\partial y}\right)^2 + \left(\frac{\partial \mathrm{u}}{\partial \mathrm{y}} + \frac{\partial \mathrm{v}}{\partial \mathrm{x}}\right)^2} \quad (2)$$

with horizontal tension strain

$$|D_T| = \sqrt{\left(\frac{\partial u}{\partial x} - \frac{\partial v}{\partial y}\right)^2} \quad (3)$$

and horizontal shearing strain

$$|D_S| = \sqrt{\left(\frac{\partial u}{\partial y} + \frac{\partial v}{\partial x}\right)^2} \quad (4)$$

297 with (u, v) being the model velocities components and (∂x, ∂y) the model grid size in longitudinal and
298 latitudinal direction, respectively. Figure 2g shows the 24.84-h averaged (two M_2 cycles) deformation
299 obtained from the CR surface currents on 15.01.2015 (the influence of the most dominant tidal
300 constituent is excluded). The order of this property O (10^{-5}) is within the ranges measured by Molinari
301 and Kirwan (1975) with Lagrangian drifters in the Caribbean Sea. The most obvious features are the
302 two large areas on the shelf exhibiting low deformation, namely, the North Sea and the Celtic Sea,
303 including the Armorican Shelf connected by the English Channel and Southern Bight, where several
304 localised high-deformation areas appear (compare Fig. 2g with 2b). High-deformation areas are also
305 present in the Irish Sea extending to the northern coast of Ireland. The difference of deformation
306 between the CR and NTE (i.e. CR minus NTE) can be related to tides and clearly shows their impact
307 on these three areas (Fig. 2h). In addition to shallow, enclosed areas, the deformation along the shelf
308 edge of the Celtic Sea is also affected by tides. High-deformation features in the deep ocean arise at the
309 eddy boundaries (compare Fig. 2g with 2a) and most of them are also present in the NTE. Hence, flow
310 deformation is expected to be of significant importance for water masses in the deep ocean. Exceptions
311 are the Bay of Biscay and the northwest of the domain where the deformation is less pronounced in the
312 NTE. The difference patterns there have scales of mesoscale eddies suggesting that these eddy dynamics
313 could be coupled to the one of tides. In the Norwegian Trench, high deformation is observed along the
314 southern 200 m isobath. Here, the influence of tides arises as small-scale patterns associated with the
315 interaction of the two currents.
316
317 *3.2 Model validation*
318 The root mean square difference of January 2015 SST of the model and OSTIA data reveals values
319 smaller than 1.5°C in vast areas of the model domain, whereas values between 0.5 and 1.0°C are the
320 typical range (Fig. S3).
321
322 Scatter plots of drifter and model velocities show a good model performance in the range of ±25
323 cm s^{-1}, where the quantile-quantile plot (qq-plot) is almost along the diagonal (Fig. S4a and S4b).
324 Deficiencies in the model occur at higher velocities, where the model is too slow probably due to the

neglected direct wind drag and Stokes drift (Röhrs et al., 2012; Stanev et al., 2019). Nevertheless, the linear correlations of the u and v velocity components of 0.88 and 0.84, respectively, between the drifters and the model and the corresponding RMSEs of 14.3 and 12.4 cm s^{-1} are considered to reflect a satisfactory model performance (Table 2).

The quality of the above numbers illustrating the model skill can be better understood if the drifter data are compared with independent observations using HF radar data. The corresponding scatter plots (Fig. S4c and S4d) do not show as much underestimation of high velocities as in the model (compare with Fig. S4a and S4b), but the spread of the data in two observations is comparable to the case of the model-data comparison (the standard deviation between the two observations is even larger than in the case of the model-data comparison). The conclusion from Table 2 is that the difference between the estimations from the model and data are not larger than that between two observations. Similar validations provided by Stanev et al. (2019) for the North Sea also demonstrate the credibility of the Lagrangian tracking approach.

Table 2: Summary of the model velocity validation performed by comparing GPS drifter velocities with the CR and HF radar velocities; the surface velocity components of the latter were interpolated to the drifter velocities. Details are given in the text. A positive bias denotes that drifter velocities are larger than the velocities of the CR or HF radar. The corresponding scatter plots are given in Fig. S4. n is the number of observations.

	Drifter – CR (n = 10,339)		**Drifter - HF radar** (n = 353)	
	u	v	u	v
RMSE [cm s^{-1}]	14.6	12.5	18.4	12.6
Linear correlation	0.88	0.84	0.91	0.87
Standard deviation [cm s^{-1}]	14.3	12.4	16.9	12.4
Bias [cm s^{-1}]	2.9	1.5	7.4	-2.0

4 Lagrangian model results

4.1 Overall analysis of trajectories and particle dynamics

The particle trajectories (Fig. 3) of the CR (experiment #1, see Table 1) show the well-known, dynamic features of the ENWS and the surrounding deep ocean. In relatively shallow areas, e.g. the English Channel, Southern Bight and Irish Sea, the surface and bottom currents are almost parallel (Fig. 3a and 3b). This is typical for tidally influenced, wind-driven shallow water circulation. Trajectories symbolising currents appear relatively thick in the areas dominated by strong tides because the large-scale presentation cannot effectively resolve small tidal excursions. This is supported by the magnified representation of the dynamics in Fig. 3c and 3d. After 12.42 h, the trajectories on the shelf present as nearly closed circles. The difference between the start and end positions on the circular loops give an estimate of the net transport, which is much smaller than the tidal excursions. The net transport rapidly increases, and the tidal excursions decrease further off-shelf beyond the 900 m isobaths, where the mesoscale dynamics are dominant. As in the case of the Eulerian visualisation of the velocity field, the 200 m isobath can be considered as the boundary separating the dynamics of the shallow and deep ocean. The meandering of the European Slope Current along the shelf edge (at ~500–2,000 m) is pronounced from the Bay of Biscay to the Goban Spur and around the Porcupine Bank (Fig. 3b). The Skagerrak and Norwegian Trench also show pronounced mesoscale dynamics (Fig. 3d).

4.2 Surface and bottom patterns of the particle distribution

Despite some similarities between the surface and bottom trajectories (Fig. 3), the particle accumulation patterns in shallow areas are considerably different (Fig. 4). To investigate these differences, the positions of the particles released in January (CR, experiment #1, see Table 1) are displayed in Fig. 4. After 1 month, the surface-released particles accumulate mainly along narrow patterns on the shelf and in the Skagerrak (Fig. 4a). In contrast, the coastal regions around Great Britain and Ireland (but also in the German Bight) can be considered divergence zones. The particle distribution in the deep ocean also shows small stripe-type patterns, especially in the southwestern part of the model domain and will be discussed in detail later (see Sect. 4.3). In the following, examples of pronounced accumulation and dispersal features are given.

There is a tendency for the bottom-released particles to leave areas with a steep bottom slope. The most obvious example is the continental slope are along the 200 m isobath from the Spanish coast around the Goban Spur and Porcupine Bank (Fig. 4b) until the Norwegian Trench. Van Aken (2001), Huthnance et al. (2009) and Guihou et al. (2018) demonstrated that slope currents, downward flows of shelf water and internal waves, respectively, dominate the dynamics of the ENWS continental slope. These processes can induce a net transport and in turn a tendency of bottom-released particles to leave the continental.

After 6 months, vast areas of the shelf and the western part of the domain become free of particles. The particles flow from the English Channel along the Frisian Front in the south and the Fair Isle Current in the north into the inner North Sea (Fig. 4c). The pattern in the Irish Sea is similar to the Frisian Front: a narrow stripe of particles in the middle of this basin is the remnant of a similar stripe from an earlier time (Fig. 4a) connecting the source of particles (in the south) to their sink (in the north). The region around the Orkney and Shetland Islands accumulates particles owing to on-shelf transport by the westerlies, which also empty the western open boundary. This region additionally receives particles from the south originating from the Irish Sea or floated around the western coast of Ireland; in both cases, these particles are sourced from the deep ocean. Likewise, the Bay of Biscay accumulates particles on time scales of several months. Bottom accumulation on the shelf occurs mainly and south of the Dogger Bank (Fig. 4d). Also the bottom trajectories (Fig. 3b) show that particles north of Dogger Bank are forced to flow around its western edge through a narrow channel into the basin to its southeast (see the bathymetry in Fig. 1) suggesting topographically influenced particle motions. Once the particles reach this basin, they can flow out only northward along its thalweg until they reach the northeastern edge of Dogger Bank (compare Fig. 4d with Fig. 1).

In the Skagerrak, the situation is as follows. At the bottom, the Norwegian Trench supplies the Skagerrak with particles from the Atlantic along its southern slope. At the surface, the Skagerrak receives particles from the Fair Isle Current, the German Bight and the Baltic Sea. Particles approaching

404 the Skagerrak can become trapped in its circular and eddy-dominated velocity pattern (Fig. 3d and 2b),
405 which extends from the surface down to the bottom (see also Rodhe, 1987; Gutow et al., 2018). In the
406 Norwegian Trench, the particle distribution has spatial variability due to the irregular mesoscale
407 dynamics therein.
408
409 *4.3 Tendencies of particle accumulation*
410 The current particle positions are not sufficiently representative of their accumulation and dispersal over
411 long periods and can lead to misinterpretations of their accumulation trends. This becomes evident by
412 comparing the particle positions after 1 month (Fig. 4a and 4b) with the NCPD for the same period (Fig.
413 5a and 5b). Although the general surface and bottom particle patterns (Fig. 4a and 4b) for January 2015
414 are comparable to the mean accumulation patterns (Fig. 5a and 5b), some features do not coincide. The
415 monthly NCPDs for all twelve months are shown in Fig. S5 and S6 for the surface- and bottom-released
416 particles, respectively. At the surface, only a few accumulation areas are visible on the annual mean
417 map (red areas in Fig. 5c); these areas are located in the Irish Sea (*1*), English Channel (*2*), Southern
418 Bight (*3*), German Bight (*4*), Skagerrak (*5*), at the Fair Isle Current (*6*) and at the northern coasts of
419 Ireland and Great Britain (*7*). Vast coastal areas have a NCPD smaller than 0.3, implying offshore
420 propagation. Despite the numbered accumulation areas and coasts prone to particle removal, most of
421 the domain shows neither particle accumulation nor removal (NCPD ≈ 1).
422
423 At the bottom, particle accumulation is highly variable in the deep ocean, but the removal of
424 particles from areas with steep topography is evident (Fig. 5d). On the shelf, the tendency of particles
425 to propagate away from coasts is smaller than for surface particles; particles even accumulate, e.g. in
426 the German Bight and along the eastern British coast (discussed in detail in Sect. 4.4). Further,
427 accumulation takes place to the south of Dogger Bank and in the Skagerrak. It is worth noting that the
428 major accumulation pattern at the surface along the Frisian Front (*3*, *4*) has as its counterpart a pattern
429 of removal at the bottom (compare Fig. 5c and Fig. 5d). Additionally, coastward of accumulation area
430 *4*, there is a removal area at the surface; in the same area, the bottom pattern shows a tendency of

accumulation. These opposite tendencies in the surface and bottom layers suggest that the vertical circulation is also important in shallow environments. The inflow along the southern slope of the Norwegian Trench appears as increased particle accumulation.

There are some prominent small-scale features (stripe-like or filament-like characteristics) in the deep ocean occurring as NCPD maxima and minima (Fig. 5a and S5) as well as particle accumulation and dispersal in the particle distribution (Fig. 4a). These features change their positions depending on mesoscale dynamics. They are reminiscent of the attributes reported by Haller and Yuan (2000), who demonstrated that particles initially located outside eddies accumulate in lines along the boundaries between them. When the averages are computed for a longer period, these filaments tend to disappear (compare Fig. 5a with 5c), which is explained by the fact that the time scales of eddy motions are substantially shorter than the annual scale. This follows from the changes in the position and occurrence of the stripe-type areas with NCPDs greater than 1 from month to month (compare the results from single months of Fig. S5). A more profound Lagrangian representation of eddies and their coherent character can be found in, e.g. Beron-Vera et al. (2018).

4.3.1 The role of tides

The difference in the January NCPDs between the CR and NTE (experiments #1 and 2, respectively, see Table 1 and Fig. 6a and 6b) demonstrates that the tidal forcing considerably affects the accumulation patterns on the shelf. At the surface, the largest differences between the two experiments occur along the East Anglia Plume/Frisian Front and along the front in the Irish Sea (Fig. 6a). Obviously, the tidal signal affects frontal-like structures. Further differences between the two experiments appear in the English Channel, around the north of Great Britain/Fair Isle Current, and at the continental slope of the Celtic Sea. In most of the remaining parts of the domain, these differences are rather small.

Nevertheless, tides also affect the accumulation of particles in the deep ocean, which is dominated by sub-basin-scale eddies, as well as other areas in the Bay of Biscay and in the Norwegian

458 Trench/Skagerrak, which are dominated by mesoscale motions. This could serve as another indication
459 of the interaction between tides and mesoscale dynamics.
460
461 The most pronounced large-scale feature in the differences observed at the sea surface is in the
462 vicinity of the shelf (Fig. 6a). At the bottom (Fig. 6b), the largest differences between the two
463 experiments occur also beyond the 200 m isobaths in the direction of the open ocean. The changing
464 sign of the difference reflects large oscillations at small scales of *O*(grid size), possibly indicating that
465 a further increase in the model resolution is needed to adequately resolve the accumulation and
466 dispersion of particles in the area of the continental slope. Bottom patterns in the North Sea are also
467 present and clearly demonstrate the importance of tides as a driver of particle accumulation there. The
468 principal patterns are similar to the surface with differences around Great Britain but the difference
469 signal is more variable. In the Southern Bight and southern North Sea the difference patterns are rather
470 distinct and follow the flanks of the Dogger Bank and the East Anglia Plume. This comparison between
471 the surface and bottom patterns indicates that, unlike the currents, which do not drastically change in
472 the vertical direction in the shallow ocean, the accumulation of particles at the bottom is different from
473 that at the sea surface. This suggests that the tides modifies the particle accumulation patterns by the
474 induced shear diffusion. This finding is supported by the influence of tides on surface deformation
475 (compare Fig. 6a and 2h), the pattern of which partly coincides with the NCPD difference.
476
477 *4.3.2 The role of wind*
478 A large part of the variability of shelf dynamics is caused by atmospheric variability (mostly on synoptic
479 time scales) (Jacob and Stanev, 2017); therefore, we will analyse the contributions of wind to the
480 accumulation and dispersion of particles in the FWE and NWE (experiments #3 and 4, respectively, see
481 Table 1). It is worth noting that the ranges of the responses to wind variability are comparable to the
482 responses to tides. The overall conclusion from the comparison among the differences in the surface
483 properties between the CR and NTE (Fig. 6a) from one perspective and between the CR and FWE (Fig.
484 6c) from another perspective is that the largest differences caused by tides and winds occur in almost
485 the same areas: the Frisian and Irish Sea Fronts, the continental slope, and the Norwegian Trench,

whereas the English Channel is less influenced in FWE. Filtering the wind (FWE) also makes the accumulation stripes "sharper", whereas the short-term wind forcing tends to "blur" the particle distribution. However, turning the wind off (NWE) changes the accumulation patterns significantly (compare Fig. 6e and 6c). The most affected areas are (1) the coastal areas of Great Britain and Ireland, (2) the Skagerrak, which no longer accumulates particles, (3) the mouths of the Rhine and Elbe rivers which extend further to the west, and (4) the coasts of the Armorican Shelf. Reducing the variability of the wind or turning it off completely also has very pronounced impacts on the bottom particles (compare Fig. 6d and 6f). The strongest impacts on bottom accumulation patterns are located in the northern part of the shelf and the Norwegian Trench/Skagerrak.

The difference between the FWE and NWE (not illustrated here) demonstrates that, on the shelf, the westerlies are essential for particle accumulation (compare Fig. 6e with 6g and Fig. 6f with 6h).

4.3.3 The role of fronts

The high-salinity and high-temperature gradients (fronts) in Fig. 2d and 2f are similar to the NCPD patterns shown in Fig. 5a. These fronts support the ones reported by Belkin et al. (2009), particularly the fronts in the southern North Sea. Additionally, in terms of the yearly averaged NCPD (Fig. 5c), the NCPD maxima coincide with the known front positions; in contrast, not all detected fronts show particle accumulation. There are also some differences from the analysis of Pietrzak et al. (2011), who analysed the dynamics of the Frisian Front and East Anglia Plume using satellite data of the SST and SPM. The differences between the present simulations and the results of Pietrzak et al. (2011) occur as a missing East Anglia Plume and are mostly because the particles in the model have a neutral buoyancy and because no particle sources are prescribed (the seeding is uniform).

To demonstrate the ability of a front to accumulate particles, a surface section across the Rhine Plume (Frisian Front) is chosen as an example (solid black line in Fig. 5a; see also its inset). The front separates the waters of the English Channel (higher salinity) and the Rhine ROFI (lower salinity). In Fig. 7, the graphs start in the west (left) and end in the east (right). The maximum NCPD in the CR (left

514 vertical dashed line) is located where the salinity and temperature start to decrease (~34.6 to 28.7 PSU
515 and ~7.6 to 5.3°C, respectively). The related density changes are ~4.62 and 0.28 kg m^{-3}. Hence, the
516 salinity causes the density gradient which in turn influences the accumulation of particles. In the
517 backward simulation (CR-B; experiment #5, see Table 1), the NCPD maximum (right vertical dashed
518 line) is at the same location with respect to the salinity change when the particles are coming from the
519 opposite direction. Due to the residual currents, in the CR the particles come from the southwest and in
520 the CR-B from the northeast. The peaks of the NCPD curves are bounded by a rather constant NCPD,
521 which is higher on the side of particle supply than on the side of particle dispersion in the CR. In the
522 CR-B, the particle supply is reduced by the front, because only particles from the German Bight and
523 the Danish coastal region can reach the front. These regions are relatively small compared to the whole
524 North Sea being the particle supplier in the CR. This implies that particle simulations in regions with
525 frontal systems are not fully reversible and backward simulations have to be interpreted carefully. In
526 terms of the position of NCPD maxima, the results of Fig. 7 are very similar to what has been found by
527 Flament and Armi (2000) and Lohmann and Belkin (2014). Despite the vertical dynamics (see Sect.
528 4.4), particle accumulation along fronts can be explained considering that the residual velocity is not
529 parallel to the front but oriented further clockwise (in the CR the orientation of the front is almost in the
530 north–south direction, whereas U is veered clockwise). This would lead to a crossing of the front by
531 particles, but the particles are hindered by the (haline) front and flow along it. In the CR-B, the dynamics
532 are reversed, and thus, particles accumulate on the other side of the front. Particle accumulation along
533 other ROFIs can also be observed at, e.g. the western Danish coast along the Elbe River outflow. Postma
534 (1984) called the boundary of the Wadden Sea a “line of no return” whose location is comparable to a
535 strong salinity gradient (Fig. 2c and 2d). From the results of the present study, this interpretation of the
536 boundary of the Wadden Sea can be confirmed: if a particle of the German Bight crosses the front, it is
537 unlikely that it will be able to return.
538
539 In the NWE (Fig. 6e), the Frisian and Irish Sea Fronts are less pronounced than in the CR,
540 demonstrating the intensification of frontal accumulation by wind. Due to the missing westerly wind,
541 particles are no longer transported to the fronts, where they can accumulate in the areas of thermohaline

gradients. This is especially true for regions where the wind is constantly blowing in the same direction, e.g. regions within the westerlies.

Another kind of shelf front is a tidal mixing front (Sect. 3.1 and Fig. S2), whose dynamics have been described repeatedly (e.g. Hill et al., 1993). These fronts are known to accumulate natural and artificial flotsam (Simpson and Pingree, 1978). In July, tidal mixing fronts are clearly visible as temperature gradients (Fig. S2a), and some of them can be observed in terms of NCPD patterns (Fig. S2c). In contrast to January, these fronts disappear in July if the tides are turned off and demonstrate their importance for particle accumulation in summer (Fig. S2d). Analyses of the January NTE results (not shown) show almost no vanishing NCPD maxima implying that these maxima are not caused by tides. Due to the seasonal occurrence, tidal mixing fronts are less pronounced in the yearly averaged NCPD then others fronts, e.g. the fronts of ROFIs. However, not all of them occur as NCPD maxima. Although the well-known jet-like velocities along fronts can be seen in U in Fig. 7, the horizontal model resolution is probably too coarse; that is, the model cannot resolve all important frontal dynamics.

4.4. Vertical circulation in the North Sea

Although shelf dynamics are dominated by strong horizontal motions, they cannot be considered fully two-dimensional. Examples of the role of vertical processes are given by tidal mixing fronts (Garret and Loder, 1981; van Aken et al, 1987), upwelling in the German Bight (Krause et al., 1986), tidal straining (de Boer et al., 2009) and secondary circulation in estuaries. The differences between the surface and bottom accumulation patterns described in Sect. 4.3.3 (Fig. 5a and 5b) are indicative of the role of vertical processes. Such indications are clearly observed in the map of the differences between the vertical positions of particles released at the bottom after one month of integration (Fig. 8a). Pronounced depth changes appear along the eastern British coast, eastern Irish coast, around the Dogger Bank and in several smaller coastal areas, e.g. at the western French coast. Some of these patterns are topographically induced, like the one at the Dogger Bank, where particles from the northwest ascend and particles released on the Dogger Bank descend. However, a NCPD at the surface smaller than 1 and a NCPD at the bottom greater than 1 (compare Fig. 5c with 5d) suggest an upward movement of

570 water not being induced by topography. Single particle trajectories along the British coast reveal that
571 the bottom flow is directed coastward and offshore at the surface (small inset in Fig. 8a).
572
573 In the backtracking experiment (CR-B, experiment #5, see Table 1; Fig. 8b), particles accumulate
574 in coastal upwelling areas, emphasising the dynamics described above. The opposite situation is present
575 on the northwestern Irish coast and in the western Irish Sea; here, a downward movement of water can
576 be observed. The NWE shows that the main driver of coastal water transport at meridionally oriented
577 coasts is the prevailing westerlies (Fig. 6e and 6f). Without wind, the eastern Irish and British coasts
578 have NCPD values clearly exceeding 0.3; with the original wind forcing, these areas have NCPD values
579 smaller than 0.3. In contrast, the NCPD of the western Irish coast and in the western Irish Sea is reduced
580 in the NWE. These results also support the theory of Lentz and Fewings (2012) regarding wind-driven
581 inner-shelf circulation.
582
583 Wind forcing is not the only explanation for the offshore-directed transport at some of the shelf
584 coasts, particularly along the eastern British coast, e.g. the Flamborough Head tidal mixing front.
585 Downwelling at fronts is associated with upwelling on the coastward side as a result of coastward
586 transport at the bottom and offshore-directed transport at the surface. Similar effects have been modelled
587 (Garret and Loder, 1981) and observed (van Aken et al., 1987) in previous studies.
588
589 *4.5 Dynamics at the shelf edge*
590 The analysis below uses the results of the CR-V (experiment #6, see Table 1) with the seeding
591 prescribed in a 100 km wide segment extending oceanward from the 150 m isobaths. The exchange of
592 particles between the deep ocean and the shelf is estimated by the number of particles crossing the 200
593 m isobaths and the changes in their depth with respect to the depth at which they were released. The
594 100 km wide segment is divided vertically into four parts: from the surface to 100 m (Fig. 9a), 100–200
595 m (Fig. 9b), 200–300 m (Fig. 9c) and 900–1,000 m (Fig. 9d). The major result of this experiment is that
596 with increasing depth (1) the dispersion of the cloud of particles in the vicinity of the 200 m isobaths
597 decreases, and (2) particles in the deeper layers do not penetrate onto the shelf. Many particles released

598 above 100 m move onto the shelf; their depth remains almost unchanged or even decreases (Fig. 9a).
599 In the three deeper intervals of release, deep oceanward transport is dominant (red stripe along the 200
600 m isobath in Fig. 9b, c and d). These dynamics, which are sketched in Fig. 9e, support the results of
601 Holt et al. (2009), Huthnance et al. (2009) and Graham et al (2018), whose simulations also showed
602 shelfward transport distinctive of the upper 150 m along the 200 m isobath; below 150 m, they found
603 deep oceanward transport. The simulated exchanges between the shelf and open ocean (the extent and
604 direction of particle propagation) are also in overall agreement with the recent results of Marsh et al.
605 (2017), who analysed drifter observations and Lagrangian simulations at the ENWS continental slope.
606 Down to 300 m, particles propagating away from the continental slope form filaments and eddy-like
607 patterns as in the Bay of Biscay; another fraction of the particles are advected within the slope current.
608 Although the latter are covered by the coloured areas, some of them are visible at the entrance of the
609 Norwegian Trench. The underlying dynamics at the ENWS continental slope are discussed in Sect. 4.1
610 and 4.2.
611
612 ## 5 Conclusions
613 Lagrangian analyses in conjunction with Eulerian analyses revealed physically distinct regimes in
614 different parts of the study area. The underlying dynamics were investigated in terms of particle
615 accumulation and removal, which were quantified by the NCPD quantity. The current knowledge about
616 shelf and shelf edge processes is extended not only by analysing specific processes but also by providing
617 a rather comprehensive description of the dynamics.
618
619 - On the shelf: Fronts act as barriers and accumulate particles. Tides affect the positions and
620 appearance of particle accumulation in frontal areas. Vertical water transport at meridionally
621 oriented coasts on the shelf is influenced by westerlies. Offshore-directed wind induces a NCPD
622 smaller than 1; the situation is reversed for onshore-directed wind.
623 - In the deep ocean: Eddies influence the particle dynamics on short time scales (individual
624 months); however, an annual mean NCPD $\approx$ 1 reveals an absence of long-term stable

accumulation areas. Tides affect the NCPD, suggesting the interaction of tides and mesoscale dynamics.

- Shelf edge (200 m isobath): The shelf edge represents a transition zone from the wind- and tidally driven shallow shelf regime to a baroclinic eddy-dominated deep ocean regime. The shelf edge shows on-shelf transport in the upper layers and downwelling-like off-shelf-directed transport below 100 m. Bottom current branches tend to remove particles from the continental slope.
- At the surface: Accumulation patterns on the shelf show high variability on monthly time scales; some accumulation areas remain stable on yearly average of monthly patterns. These long-term stable zones occur mainly along the fronts of ROFIs and in the Skagerrak. In the Bay of Biscay accumulation patterns form on longer time scales than one month. At the shelf edge, particles are transported onto the shelf by westerlies. The influence of wind on particle accumulation is on the order of the influence of tides.
- At the bottom: On the shelf, bottom currents are mainly influenced by the topography and follow its thalweg.

The differences in the properties of the velocity field (e.g. deformation) reveal two different regimes: a shelf regime with rather little deformation and a deep ocean regime with considerable deformation. On the shelf, tidally induced deformation plays an important role in particle accumulation and dispersal.

The present study demonstrates the illustrative potential of Lagrangian methods. In conjunction with traditional Eulerian analysis, Lagrangian analysis can enhance the interpretation of observed or simulated dynamics and provide a solid basis for estimating the propagation of floating marine debris.

Code/data availability: The model codes of NEMO (https://www.nemo-ocean.eu), ARIANE (stockage.univ-brest.fr/~grima/Ariane/) and OpenDrift (https://github.com/OpenDrift/opendrift) as

well as the GPS drifter (Carrasco and Horstmann, 2017), HF radar (http://codm.hzg.de/codm/) and OSTIA data (marine.copernicus.eu) are freely available. Scripts and model data can be obtained by a request to the corresponding author.

Author contributions. MR and EVS conceived the study. MR performed the model runs and analysed and prepared the figures. MR and EVS interpreted the results, and MR prepared the manuscript with a significant contribution from EVS.

Competing interests. The authors declare that they have no conflicts of interest.

Acknowledgments. We thank the UK Met Office and Joanna Staneva for providing the NEMO AMM7 setup. This study was carried out within the project "Macroplastics Pollution in the Southern North Sea – Sources, Pathways and Abatement Strategies" (grant no. ZN3176) funded by the German Federal State of Lower Saxony. The authors thank Sebastian Grayek for technical support and Jens Meyerjürgens for carefully reading the manuscript and giving important advice. We appreciate the two anonymous reviewers for their critical and detailed comments.

References

van Aken, H. M. (2001). The hydrography of the mid-latitude Northeast Atlantic Ocean — Part III: the subducted thermocline water mass. *Deep Sea Res. Pt. I: Oceanographic Research Papers*, *48*(1), 237–267. https://doi.org/10.1016/S0967-0637(00)00059-5

van Aken, H. M., van Heijst, G. J. F., & Maas, L. R. M. (1987). Observations of fronts in the North Sea. *J. Mar. Res.*, *45*(3), 579–600. https://doi.org/10.1357/002224087788326830

Backhaus, J. (1979). First Results of a Three-Dimensional Model on the Dynamics in the German Bighta. In J. C. J. Nihoul (Ed.), *Elsev. Oceanogr. Serie.* (Vol. 25, pp. 333–349). Elsevier. https://doi.org/10.1016/S0422-9894(08)71138-3

679 Backhaus, J. O. (1985). A three-dimensional model for the simulation of shelf sea dynamics.
680 *Deutsche Hydrografische Zeitschrift*, *38*(4), 165–187. https://doi.org/10.1007/BF02328975
681 Baschek, B., Schroeder, F., Brix, H., Riethmuller, R., Badewien, T.H., Breitbach, G., et al. (2017).
682 The coastal observing system for northern and arctic seas (COSYNA). Ocean Sci. *13*(3), 379–
683 410. https://doi.org/10.5194/os-13-379-2107
684 Belkin, I. M., Cornillon, P. C., & Sherman, K. (2009). Fronts in Large Marine Ecosystems. *Prog.*
685 *Oceanogr.*, *81*(1), 223–236. https://doi.org/10.1016/j.pocean.2009.04.015
686 Beron-Vera, F. J., Hadjighasem, A., Xia, Q., Olascoaga, M. J., & Haller, G. (2018). Coherent
687 Lagrangian swirls among submesoscale motions. *P. Natl. Acad. Sci. USA*, 201701392.
688 https://doi.org/10.1073/pnas.1701392115
689 Blanke, B., & Raynaud, S. (1997). Kinematics of the Pacific Equatorial Undercurrent: An Eulerian
690 and Lagrangian Approach from GCM Results. *J. Phys. Oceanogr.*, *27*(6), 1038–1053.
691 https://doi.org/10.1175/1520-0485(1997)027<1038:KOTPEU>2.0.CO;2
692 Blanke, B., Arhan, M., Madec, G., & Roche, S. (1999). Warm Water Paths in the Equatorial Atlantic
693 as Diagnosed with a General Circulation Model. *J. Phys. Oceanogr.*, *29*(11), 2753–2768.
694 https://doi.org/10.1175/1520-0485(1999)029<2753:WWPITE>2.0.CO;2
695 de Boer, G. J., Pietrzak, J. D., & Winterwerp, J. C. (2009). SST observations of upwelling induced by
696 tidal straining in the Rhine ROFI. *Cont. Shelf Res.*, *29*(1), 263–277.
697 https://doi.org/10.1016/j.csr.2007.06.011
698 Booth, D. A. (1988). Eddies in the Rockall Trough. *Oceanologica Acta*, *11*(3), 213–219.
699 Bower, A. S., Lozier, M. S., Gary, S. F., & Böning, C. W. (2009). Interior pathways of the North
700 Atlantic meridional overturning circulation. *Nature*, *459*(7244), 243–247.
701 https://doi.org/10.1038/nature07979
702 Brown, J., Hill, A. E., Fernand, L., & Horsburgh, K. J. (1999). Observations of a Seasonal Jet-like
703 Circulation at the Central North Sea Cold Pool Margin. *Estuar. Coast. Shelf S.*, *48*(3), 343–355.
704 https://doi.org/10.1006/ecss.1999.0426
705 Brown, J., Carrillo, L., Fernand, L., Horsburgh, K. J., Hill, A. E., Young, E. F., & Medler, K. J.
706 (2003). Observations of the physical structure and seasonal jet-like circulation of the Celtic Sea

and St. George's Channel of the Irish Sea. *Cont.l Shelf Res.*, *23*(6), 533–561. https://doi.org/10.1016/S0278-4343(03)00008-6

Callies, U., Plüß, A., Kappenberg, J., & Kapitza, H. (2011). Particle tracking in the vicinity of Helgoland, North Sea: a model comparison. *Ocean Dynam.*, *61*(12), 2121–2139. https://doi.org/10.1007/s10236-011-0474-8

Callies, U., Groll, N., Horstmann, J., Kapitza, H., Klein, H., Maßmann, S., & Schwichtenberg, F. (2017). Surface drifters in the German Bight: model validation considering windage and Stokes drift. *Ocean Science*, *13*(5), 799–827. https://doi.org/10.5194/os-13-799-2017

Carrasco, R., & Horstmann, J. (2017). *German Bight surface drifter data from Heincke cruise HE 445, 2015*, PANGAEA. https://doi.org/10.1594/PANGAEA.874511

Daewel, U., Peck, M. A., Kühn, W., St. John, M. A., Alekseeva, I., & Schrum, C. (2008). Coupling ecosystem and individual-based models to simulate the influence of environmental variability on potential growth and survival of larval sprat (Sprattus sprattus L.) in the North Sea. *Fish. Oceanogr.*, *17*(5), 333–351. https://doi.org/10.1111/j.1365-2419.2008.00482.x

Dagestad, K.-F., Röhrs, J., Breivik, Ø., & Ådlandsvik, B. (2018). OpenDrift v1.0: a generic framework for trajectory modelling. *Geosci. Model Dev.*, *11*(4), 1405–1420. https://doi.org/10.5194/gmd-11-1405-2018

Davies, A. M, & Xing, J. (2001). Modelling processes influencing shelf edge currents, mixing, across shelf exchange, and sediment movement at the shelf edge. *Dynam. Atmos. Oceans*, *34*(2), 291–326. https://doi.org/10.1016/S0377-0265(01)00072-0

Davies, A. M., Sauvel, J., & Evans, J. (1985). Computing near coastal tidal dynamics from observations and a numerical model. *Cont. Shelf Res.*, *4*(3), 341–366. https://doi.org/10.1016/0278-4343(85)90047-0

Donlon, C. J., Martin, M., Stark, J., Roberts-Jones, J., Fiedler, E., & Wimmer, W. (2012). The Operational Sea Surface Temperature and Sea Ice Analysis (OSTIA) system. *Remote Sensing of Environment*, *116*, 140–158. https://doi.org/10.1016/j.rse.2010.10.017

733 Flament, P., & Armi, L. (2000). The Shear, Convergence, and Thermohaline Structure of a Front.
734 *Journal of Physical Oceanography*, *30*(1), 51–66. https://doi.org/10.1175/1520-
735 0485(2000)030<0051:TSCATS>2.0.CO;2
736 Froyland, G., Stuart, R. M., & van Sebille, E. (2014). How well-connected is the surface of the global
737 ocean? *Chaos*, *24*(3), 033126. https://doi.org/10.1063/1.4892530
738 Garrett, C. J. R., & Loder, J. W. (1981). Circulation and fronts in continental shelf seas - Dynamical
739 aspects of shallow sea fronts. *Philos. T. Roy. Soc. A*, *302*(1472), 563–581.
740 https://doi.org/10.1098/rsta.1981.0183
741 Graham, J. A., Rosser, J. P., O'Dea, E., & Hewitt, H. T. (2018). Resolving Shelf Break Exchange
742 Around the European Northwest Shelf. *Geophysical Research Letters*, *45*(22), 12,386-12,395.
743 https://doi.org/10.1029/2018GL079399
744 Guihou, K., Polton, J., Harle, J., Wakelin, S., O'Dea, E., & Holt, J. (2018). Kilometric Scale
745 Modeling of the North West European Shelf Seas: Exploring the Spatial and Temporal Variability
746 of Internal Tides. *J. Geophys. Res.-Oceans*, *122*. https://doi.org/10.1002/2017JC012960
747 Gutow, L., Ricker, M., Holstein, J., Dannheim, J., Stanev, E. V. & Wolff, J.-O. (2018). Distribution
748 and trajectories of floating and benthic marine macrolitter in the south-eastern North Sea. *Mar.*
749 *Pollut. Bull.*, *131*, *Part A*, 763–772. https://doi.org/10.1016/j.marpolbul.2018.05.003
750 Hainbucher, D., Pohlmann, T., & Backhaus, J. (1987). Transport of conservative passive tracers in the
751 North Sea: first results of a circulation and transport model. *Cont. Shelf Res.*, *7*(10), 1161–1179.
752 https://doi.org/10.1016/0278-4343(87)90083-5
753 Haller, G., & Yuan, G. (2000). Lagrangian coherent structures and mixing in two-dimensional
754 turbulence. *Physica D*, *147*(3), 352–370. https://doi.org/10.1016/S0167-2789(00)00142-1
755 Heaps, N. S. (1980). Density currents in a two-layered coastal system, with application to the
756 Norwegian Coastal Current. *Geophys. J. Roy. Astr. S.*, *63*(2), 289–310.
757 https://doi.org/10.1111/j.1365-246X.1980.tb02622.x
758 Hill, A. E., James, I. D., Linden, P. F., Matthews, J. P., Prandle, D., Simpson, J. H., et al. (1993).
759 Understanding the North Sea system - Dynamics of tidal mixing fronts in the North Sea. *Philos.*
760 *T. Roy. Soc. A*, *343*(1669), 431–446. https://doi.org/10.1098/rsta.1993.0057

761 Hill, A. E., Brown, J., Fernand, L., Holt, J., Horsburgh, K. J., Proctor, R., Raine, R., & Turrell, W. R.
762 (2008). Thermohaline circulation of shallow tidal seas. *Geophys. Res. Lett.*, *35*(11), L11605.
763 https://doi.org/10.1029/2008GL033459
764 Holmström, A. (1975). Plastic films on the bottom of the Skagerack. *Nature*, *255*(5510), 622–623.
765 https://doi.org/10.1038/255622a0
766 Holt, J. T., & James, I. D. (1999). A simulation of the Southern North Sea in comparison with
767 measurements from the North Sea Project. Part 1: Temperature. *Cont. Shelf Res.*, *19*(8), 1087–
768 1112. https://doi.org/10.1016/S0278-4343(99)00015-1
769 Holt, J., & Umlauf, L. (2008). Modelling the tidal mixing fronts and seasonal stratification of the
770 Northwest European Continental shelf. *Cont. Shelf Res.*, *28*(7), 887–903.
771 https://doi.org/10.1016/j.csr.2008.01.012
772 Holt, J., Wakelin, S., & Huthnance, J. (2009). Down-welling circulation of the northwest European
773 continental shelf: A driving mechanism for the continental shelf carbon pump. *Geophysical*
774 *Research Letters*, *36*(14), L14602. https://doi.org/10.1029/2009GL038997
775 Howarth, M. J. (2001). North Sea Circulation. In J. H. Steele, K. K. Turekian, & S. A. Thorpe (Eds.),
776 *Encyclopedia of Ocean Sciences: Vol. 1* (1st edition, pp. 1912–1921). Oxford: Academic Press.
777 Huntley, H. S., Lipphardt, B. L., Jacobs, G., & Kirwan, A. D. (2015). Clusters, deformation, and
778 dilation: Diagnostics for material accumulation regions. *Journal of Geophysical Research:*
779 *Oceans*, *120*(10), 6622–6636. https://doi.org/10.1002/2015JC011036
780 Huthnance, J. M. (1991). Physical oceanography of the North Sea. *Ocean and Shoreline Management*,
781 *16*(3), 199–231. https://doi.org/10.1016/0951-8312(91)90005-M
782 Huthnance, J. M. (1995). Circulation, exchange and water masses at the ocean margin: the role of
783 physical processes at the shelf edge. *Prog. Oceanogr., 35*(4), 353–431.
784 https://doi.org/10.1016/0079-6611(95)80003-C
785 Huthnance, J. M., Holt, J. T., & Wakelin, S. L. (2009). Deep ocean exchange with west-European
786 shelf seas. *Ocean Sci.*, *5*(4), 621–634. https://doi.org/10.5194/os-5-621-2009
787 Jacob, B., & Stanev, E. V. (2017). Interactions between wind and tidally induced currents in coastal
788 and shelf basins. *Ocean Dynam.*, *67*(10), 1263–1281. https://doi.org/10.1007/s10236-017-1093-9

789 Jacobs, G. A., Huntley, H. S., Kirwan, A. D., Lipphardt, B. L., Campbell, T., Smith, T., Edwards, K.,
790 & Bartels, B. (2016). Ocean processes underlying surface clustering. *J. Geophys. Res. Oceans*,
791 *121*(1), 180–197. https://doi.org/10.1002/2015JC011140
792 Krause, G., Budeus, G., Gerdes, D., Schaumann, K., & Hesse, K. (1986). Frontal Systems in the
793 German Bight and their Physical and Biological Effects. In J. C. J. Nihoul (Ed.), *Elsev. Oceanogr.*
794 *Serie.* (Vol. 42, pp. 119–140). Elsevier. https://doi.org/10.1016/S0422-9894(08)71042-0
795 Koszalka, I. M., & LaCasce, J. H. (2010). Lagrangian analysis by clustering. *Ocean Dynam.*, *60*(4),
796 957–972. https://doi.org/10.1007/s10236-010-0306-2
797 Koszalka, I. M., LaCasce, J. H., Andersson, M., Orvik, K. A., & Mauritzen, C. (2011). Surface
798 circulation in the Nordic Seas from clustered drifters. *Deep Sea Research Part I: Oceanographic*
799 *Research Papers*, *58*(4), 468–485. https://doi.org/10.1016/j.dsr.2011.01.007
800 Le Fèvre, J. (1986). Aspects of the Biology of Frontal Systems. *Adv. Mar. Biol.*, *23*, 163–299.
801 Lentz, S. J., & Fewings, M. R. (2012). The wind- and wave-driven inner-shelf circulation. *Annu. Rev.*
802 *Mar. Sci.*, *4*(1), 317–343. https://doi.org/10.1146/annurev-marine-120709-142745
803 Lohmann, R., & Belkin, I. M. (2014). Organic pollutants and ocean fronts across the Atlantic Ocean:
804 A review. *Prog. Oceanogr.*, *128*(Supplement C), 172–184.
805 https://doi.org/10.1016/j.pocean.2014.08.013
806 Madec, G. (2008). NEMO ocean engine. *Note du Pôle de modélisation, Institut Pierre-Simon Laplace*
807 *(IPSL), France*, (27).
808 Mahadevan, A. (2016). The Impact of Submesoscale Physics on Primary Productivity of Plankton.
809 *Annu. Rev. Mar. Sci.*, *8*, 161–184. https://doi.org/10.1146/annurev-marine-010814-015912
810 Maier-Reimer, E. (1977). Residual circulation in the North Sea due to the M2-tide and mean annual
811 wind stress. *Deutsche Hydrografische Zeitschrift*, *30*(3), 69–80.
812 https://doi.org/10.1007/BF02227045
813 Marsh, R., Haigh, I. D., Cunningham, S. A., Inall, M. E., Porter, M., & Moat, B. I. (2017). Large-
814 scale forcing of the European Slope Current and associated inflows to the North Sea. *Ocean Sci.*,
815 *13*(2), 315–335. https://doi.org/10.5194/os-13-315-2017

816 Maximenko, N., Hafner, J., Kamachi, M., & MacFadyen, A. (2018). Numerical simulations of debris
817 drift from the Great Japan Tsunami of 2011 and their verification with observational reports. *Mar.*
818 *Pollut. Bull.*, *132*, 5–25. https://doi.org/10.1016/j.marpolbul.2018.03.056
819 McWilliams, J. C. (2016). Submesoscale currents in the ocean. *P. Roy. Soc. A-Math. Phy.*, *472*(2189),
820 20160117. https://doi.org/10.1098/rspa.2016.0117
821 van der Molen, J., García-García, L. M., Whomersley, P., Callaway, A., et al. (2018). Connectivity of
822 larval stages of sedentary marine communities between hard substrates and offshore structures in
823 the North Sea. *Scientific Reports*, *8*(1), 14772. https://doi.org/10.1038/s41598-018-32912-2
824 Molinari, R., & Kirwan, A. D. (1975). Calculations of Differential Kinematic Properties from
825 Lagrangian Observations in the Western Caribbean Sea. *J. Phys. Oceanogr.*, *5*(3), 483–491.
826 https://doi.org/10.1175/1520-0485(1975)005<0483:CODKPF>2.0.CO;2
827 Neumann, D., Callies, U., & Matthies, M. (2014). Marine litter ensemble transport simulations in the
828 southern North Sea. *Mar. Pollut. Bull.*, *86*(1), 219–228.
829 https://doi.org/10.1016/j.marpolbul.2014.07.016
830 O'Dea, E. J., Arnold, A. K., Edwards, K. P., Furner, R., Hyder, P., Martin, M. J., Siddorn, J. R., et al.
831 (2012). An operational ocean forecast system incorporating NEMO and SST data assimilation for
832 the tidally driven European North-West shelf. *J. Oper. Oceanogr.*, *5*(1), 3–17.
833 https://doi.org/10.1080/1755876X.2012.11020128
834 O'Dea, E. J., Furner, R., Wakelin, S., Siddorn, J., While, J., Sykes, P., et al. (2017). The CO5
835 configuration of the 7 km Atlantic Margin Model: large-scale biases and sensitivity to forcing,
836 physics options and vertical resolution. *Geosci. Model Dev.*, *10*(8), 2947–2969.
837 https://doi.org/10.5194/gmd-10-2947-2017
838 Onink, V., Wichmann, D., Delandmeter, P., & Van Sebille, E. (n.d.). The Role of Ekman Currents,
839 Geostrophy, and Stokes Drift in the Accumulation of Floating Microplastic. *J. Geophys. Res.-*
840 *Oceans*, *124*(3), 1474–1490. https://doi.org/10.1029/2018JC014547
841 Otto, L., Zimmerman, J. T. F., Furnes, G. K., Mork, M., Saetre, R., & Becker, G. (1990). Review of
842 the physical oceanography of the North Sea. *Neth. J. Sea Res.*, *26*(2), 161–238.
843 https://doi.org/10.1016/0077-7579(90)90091-T

844 Paparella, F., Babiano, A., Basdevant, C., Provenzale, A., & Tanga, P. (1997). A Lagrangian study of
845 the Antarctic polar vortex. *J. Geophys. Res.-Atmos.*, *102*(D6), 6765–6773.
846 https://doi.org/10.1029/96JD03377
847 Pätsch, J., Burchard, H., Dieterich, C., Gräwe, U., Gröger, M., Mathis, M., et al. (2017). An
848 evaluation of the North Sea circulation in global and regional models relevant for ecosystem
849 simulations. *Ocean Model.*, *116*(Supplement C), 70–95.
850 https://doi.org/10.1016/j.ocemod.2017.06.005
851 Pietrzak, J. D., de Boer, G. J., & Eleveld, M. A. (2011). Mechanisms controlling the intra-annual
852 mesoscale variability of SST and SPM in the southern North Sea. *Cont. Shelf Res.*, *31*(6), 594–
853 610. https://doi.org/10.1016/j.csr.2010.12.014
854 Pingree, R. D., & Griffiths, D. K. (1978). Tidal fronts on the shelf seas around the British Isles. *J.*
855 *Geophys. Res.-Oceans*, *83*(C9), 4615–4622. https://doi.org/10.1029/JC083iC09p04615
856 Pohlmann, T. (2006). A meso-scale model of the central and southern North Sea: Consequences of an
857 improved resolution. *Cont. Shelf Res.*, *26*(19), 2367–2385.
858 https://doi.org/10.1016/j.csr.2006.06.011
859 Porter, M., Inall, M. E., Green, J. A. M., Simpson, J. H., Dale, A. C., & Miller, P. I. (2016). Drifter
860 observations in the summer time Bay of Biscay slope current. *Journal of Marine Systems*, *157*,
861 65–74. https://doi.org/10.1016/j.jmarsys.2016.01.002
862 Postma, H. (1984). Introduction to the symposium on organic matter in the Wadden Sea. In R. W. P.
863 M. Laane & W. J. Wolff (Eds.), *The role of organic matter in the Wadden Sea* (pp. 15–22). Texel,
864 Netherlands.
865 Reisser, J., Shaw, J., Wilcox, C., Hardesty, B. D., Proietti, M., Thums, M., & Pattiaratchi, C. (2013).
866 Marine Plastic Pollution in Waters around Australia: Characteristics, Concentrations, and
867 Pathways. *PLOS ONE*, *8*(11), e80466. https://doi.org/10.1371/journal.pone.0080466
868 Rodhe, J. (1987). The large-scale circulation in the Skagerrak; interpretation of some observations.
869 *Tellus A*, *39A*(3), 245–253. https://doi.org/10.1111/j.1600-0870.1987.tb00305.x

Röhrs, J., Christensen, K. H., Hole, L. R., Broström, G., Drivdal, M., & Sundby, S. (2012). Observation-based evaluation of surface wave effects on currents and trajectory forecasts. *Ocean Dynam.*, *62*(10–12), 1519–1533. https://doi.org/10.1007/s10236-012-0576-y

Rolinski, S. (1999). On the dynamics of suspended matter transport in the tidal river Elbe: Description and results of a Lagrangian model. *J. Geophys. Res.-Oceans*, *104*(C11), 26043–26057. https://doi.org/10.1029/1999JC900230

Schönfeld, W. (1995). Numerical simulation of the dispersion of artificial radionuclides in the English Channel and the North Sea. *J. Marine Syst.*, *6*(5), 529–544. https://doi.org/10.1016/0924-7963(95)00022-H

van Sebille, E., England, M. H., & Froyland, G. (2012). Origin, dynamics and evolution of ocean garbage patches from observed surface drifters. *Environmental Research Letters*, *7*(4), 044040. https://doi.org/10.1088/1748-9326/7/4/044040

van Sebille, E., Wilcox, C., Lebreton, L., Maximenko, N., Hardesty, B. D., van Franeker, J. A., et al. (2015). A global inventory of small floating plastic debris. *Environmental Research Letters*, *10*(12), 124006. https://doi.org/10.1088/1748-9326/10/12/124006

van Sebille, E., Griffies, S. M., Abernathey, R., Adams, T. P., Berloff, P., Biastoch, A., Blanke, B., et al. (2018). Lagrangian ocean analysis: Fundamentals and practices. *Ocean Model.*, *121*, 49–75. https://doi.org/10.1016/j.ocemod.2017.11.008

Simpson, J. H., & Hunter, J. R. (1974). Fronts in the Irish Sea. *Nature*, *250*(5465), 404–406. https://doi.org/10.1038/250404a0

Simpson, J. H., & Pingree, R. D. (1978). Shallow Sea Fronts Produced by Tidal Stirring. In *Oceanic Fronts in Coastal Processes* (pp. 29–42). Berlin: Springer. https://doi.org/10.1007/978-3-642-66987-3_5

Simpson, J. H., & Sharples, J. (2012). *Introduction to the Physical and Biological Oceanography of Shelf Seas*. Cambridge: Cambridge University Press.

Smagorinsky, J. (1963). General circulation experiments with the primitive equations. *Mon. Weather Rev.*, *91*(3), 99–164. https://doi.org/10.1175/1520-0493(1963)091<0099:GCEWTP>2.3.CO;2

Stanev, E. V., & Ricker, M. (2020). Interactions between barotropic tides and mesoscale processes in deep ocean and shelf regions. Accepted in *Ocean Dynam.*

Stanev, E. V., Schulz-Stellenfleth, J., Staneva, J., Grayek, S., Grashorn, S., Behrens, A., Koch, W. & Pein, J. (2016). Ocean forecasting for the German Bight: from regional to coastal scales. *Ocean Sci.*, *12*(5), 1105–1136. https://doi.org/10.5194/os-12-1105-2016

Stanev, E. V., Badewien, T. H., Freund, H., Grayek, S., Hahner, F., Meyerjürgens, J., Ricker, M., et al. (2019). Extreme westward surface drift in the North Sea: Public reports of stranded drifters and Lagrangian tracking. *Cont. Shelf Res.*, *177*, 24–32. https://doi.org/10.1016/j.csr.2019.03.003

Stanev, E. V., Ziemer, F., Schulz-Stellenfleth, J., Seemann, J., Staneva, J., & Gurgel, K. W. (2015). Blending Surface Currents from HF Radar Observations and Numerical Modelling: Tidal Hindcasts and Forecasts, *J. Atmos. Ocean. Tech.*, *32*(2), 256–281. https://doi.org/10.1175/JTECH-D-13-00164.1

Wakata, Y., & Sugimori, Y. (1990). Lagrangian Motions and Global Density Distributions of Floating Matter in the Ocean Simulated Using Shipdrift Data. *J. Phys. Oceanogr.*, *20*(1), 125–138. https://doi.org/10.1175/1520-0485(1990)020<0125:LMAGDD>2.0.CO;2

Zhang, Y. J., Stanev, E. V., & Grashorn, S. (2016). Unstructured-grid model for the North Sea and Baltic Sea: Validation against observations. *Ocean Model.*, *97*, 91–108. https://doi.org/10.1016/j.ocemod.2015.11.009

915 **Figure captions:**

916 **Fig. 1**. Bathymetry of the model domain. The shelf is defined as depths shallower than 200 m (colour
917 bar within the map). In this and all following figures, the 200 m depth contour is highlighted with a
918 black solid line. Grey arrows in schematically show the general shelf sea circulation. The
919 abbreviations used in the text are as follows:
920 Armorican Shelf (*AS*), Bay of Biscay (*BB*), Celtic Sea (*CS*), Dogger Bank (*DB*), East Anglia (*EA*),
921 English Channel (*EC*), German Bight (*GB*), Goban Spur (*GS*), Irish Sea (*IS*), Kattegat (*Ka*), North Sea
922 (*NS*), Norwegian Trench (*NT*), Rockall Trough (*RT*), Skagerrak (*Sk*), Southern Bight (*SB*), St.
923 George's Channel (*SGC*), Orkney/Shetland Islands (*OI*/*SI*), Outer Hebrides (*OH*), Porcupine Bank
924 (*PB*), Fair Isle Current (*a*), European Slope Current (*b*), East Anglia Plume (*c*), Frisian Front (*d*),
925 Rhine River (*1*), Ems River (*2*), Weser River (*3*) and Elbe River (*4*).
926
927 **Fig. 2.** Simulated surface properties in the control run (CR, #1, see Table 1) for January 2015: (a)
928 velocity magnitude derived from the averaged u and v velocity components, (b) mean velocity
929 magnitude, (c) mean salinity and (e) mean temperature. Magnitudes of the (d) temperature and (f)
930 salinity gradients as well as (g) the deformation in the CR and (h) the differences CR minus the
931 nontidal experiment (NTE, #2) of the deformation are presented as 24.84-h averaged fields on 15
932 January 2015.
933
934 **Fig. 3**. Lagrangian trajectories of every 8th particle after 15 days of integration in the control run (CR,
935 #1, see Table 1) released on 01 January 2015. Particles are released at (a) the surface and (b) bottom.
936 (c) and (d) are magnified views of the domain showing all trajectories of (c) the first 12.42 h and (d)
937 24 h representative of different dynamics: (c) the area of the Armorican Shelf continental slope
938 including tidal ellipses and (d) the circulation in the Skagerrak. The trajectory colours are randomly
939 chosen for better visibility. Grey lines are isobaths in (c) 700-m and (d) 400-m steps.
940
941 **Fig. 4**. Particle positions after (a, b) 1 month and (c, d) 6 months released on 01 January 2015 at (a, c)
942 the surface and (b, d) bottom in the control run (CR, #1, see Table 1).

Fig. 5. Tendencies of accumulation shown as (a, b) the January mean normalised cumulative particle density (NCPD) and (c, d) the average of monthly NCPD for 2015 (averages of Fig. S5 and S6, respectively) in the control run (CR, #1, see Table 1). (a) and (c) correspond to surface-released particles, while (b) and (d) correspond to bottom-released particles . In (a), the solid black line located in the Southern Bight is the transect shown in Fig. 7 (enlarged in the inset). The numbers in (c) indicate the most pronounced accumulation areas.

Fig. 6. Analysis of the sensitivity experiments with respect to tides and wind. (a) and (b) are the differences of normalised cumulative particle density (NCPD) in the control run (CR, #1, see Table 1) minus the nontidal experiment (NTE, #2) in January 2015 at (a) the surface and (b) bottom. (c) and (d) are the corresponding differences between the CR and filtered wind experiment (FWE, #3); (e) and (f) are the differences between the CR and nonwind wind experiment (NWE, #4).

Fig. 7. Normalised cumulative particle density (NCPD), salinity (S), temperature (T) and residual velocity vectors (U) at the surface as the means of January 2015 along the transect in the Southern Bight (solid black line in Fig. 5a) in the control run (CR). The graph starts in the west and ends at the coast. The vertical dotted lines mark the NCPD maxima of the forward (left one, solid NCPD line) and backward (right one, dashed NCPD line) simulations (CR and CR-B, #1 and 5, respectively, see Table 1).

Fig. 8. (a) Difference of the final depth minus the initial depth of bottom-released particles after 1 month (January) in 2015 in the control run (CR, #1, see Table 1). Positive/negative values indicate a depth increase/decrease. The model grid in which a particle was released is coloured depending on its depth change. The small figure shows a magnified view of the British coast with two exemplary bottom (black) and surface (red) trajectories starting at the big dots. The trajectories are detided with a 25-h flowing mean. (b) Tendencies of accumulation shown as the January mean normalised cumulative particle density NCPD calculated from the backward simulation (CR-B, #5).

Fig. 9. Particle positions (purple dots) and particle depth differences with respect to the depth of release in different depth layers (colours) after 1 month (January) in 2015 computed in the control run with vertical particle seeding along the continental slope (CR-V, #6, see Table 1). Details of the seeding strategy can be found in Sect. 2.3. The colour coding shows the difference of the final depth minus the initial particle depth, computed as the mean difference of all particle depths seeded at the same location in the horizontal plane. All particles released in the respective depth range are taken into account. Particles were released in four depth layers: (a) 1–100 m, (b) 100–200 m, (c) 200–300 m and (d) 900–1,000 m. (e) Sketched dynamics at the continental slope concluded from (a) to (d).

Figures:

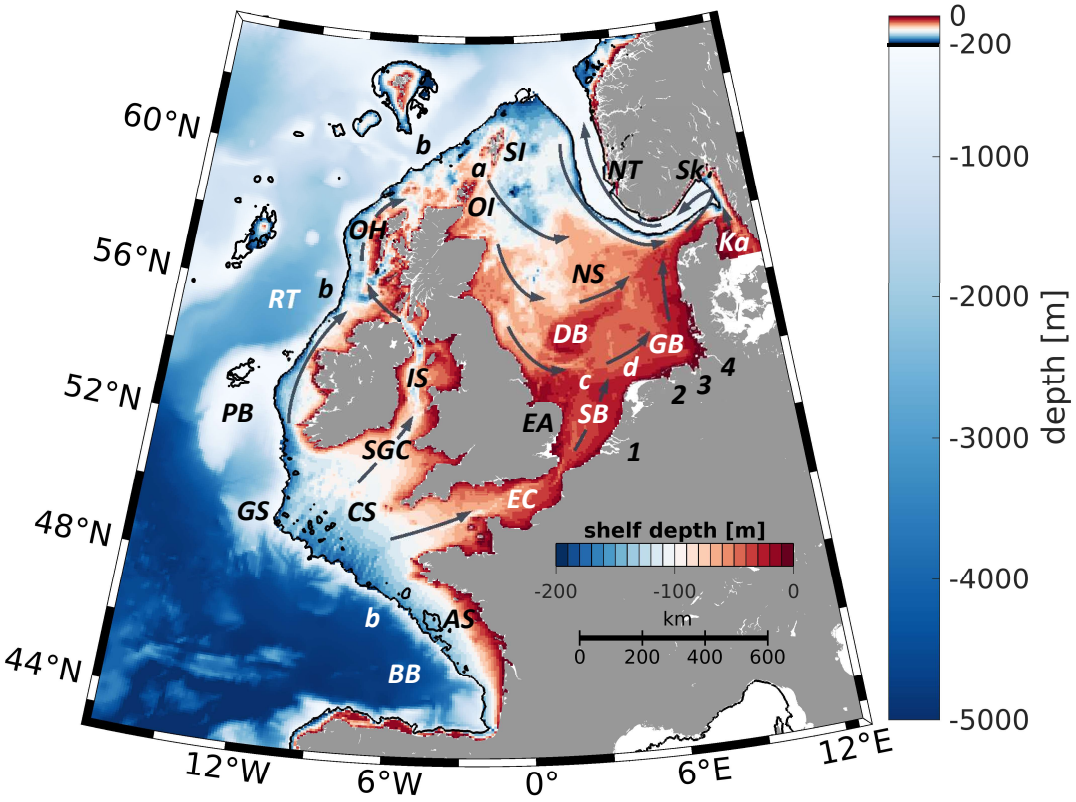

Fig. 1.

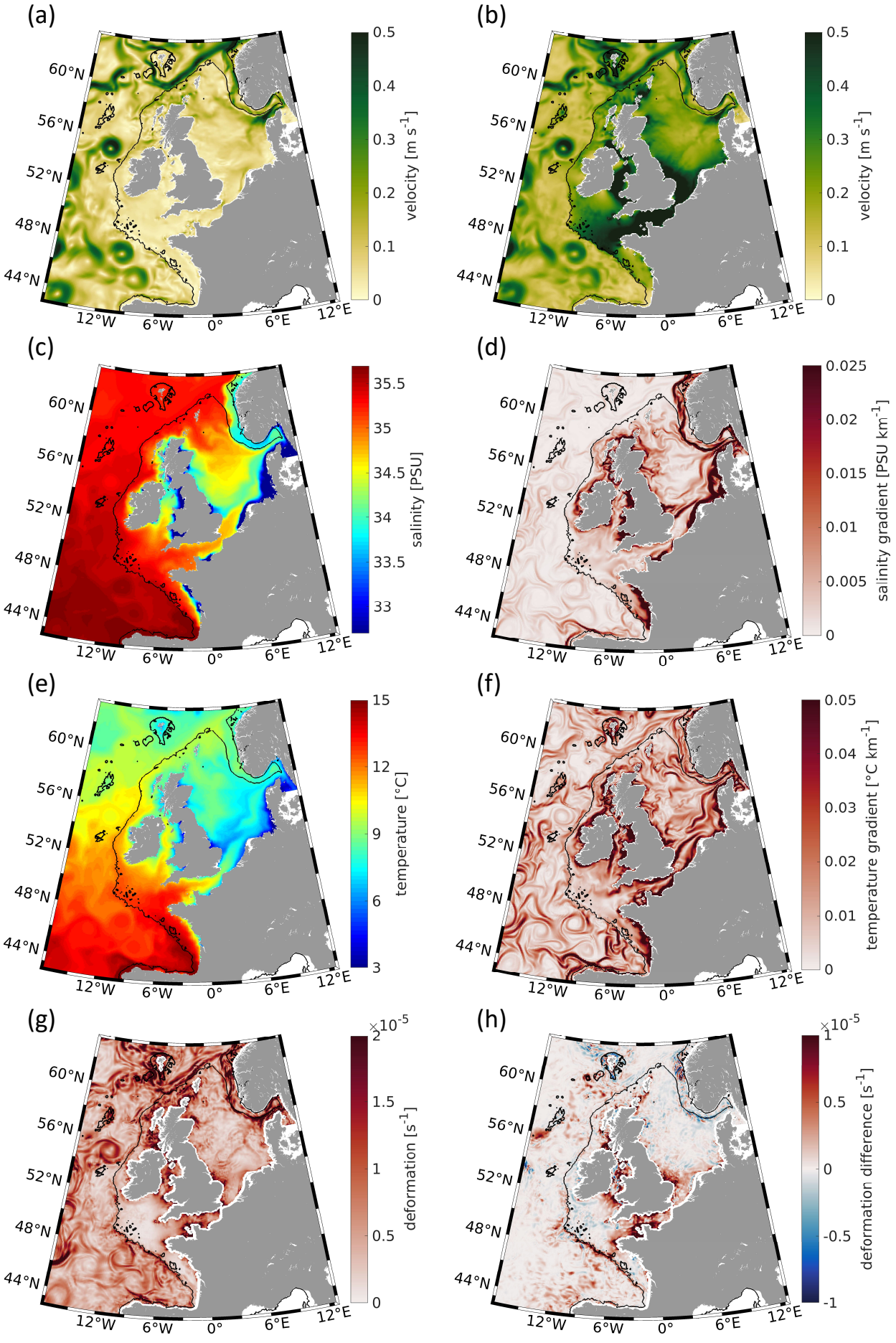
(a)
(b)
(c)
(d)
(e)
(f)
(g)
(h)
60°N
56°N
52°N
48°N
44°N
12°W
6°W
0°
6°E
12°E
velocity [m s-1]
salinity [PSU]
salinity gradient [PSU km-1]
temperature [°C]
temperature gradient [°C km-1]
deformation [s-1]
deformation difference [s-1]
×10-5

Fig. 2.

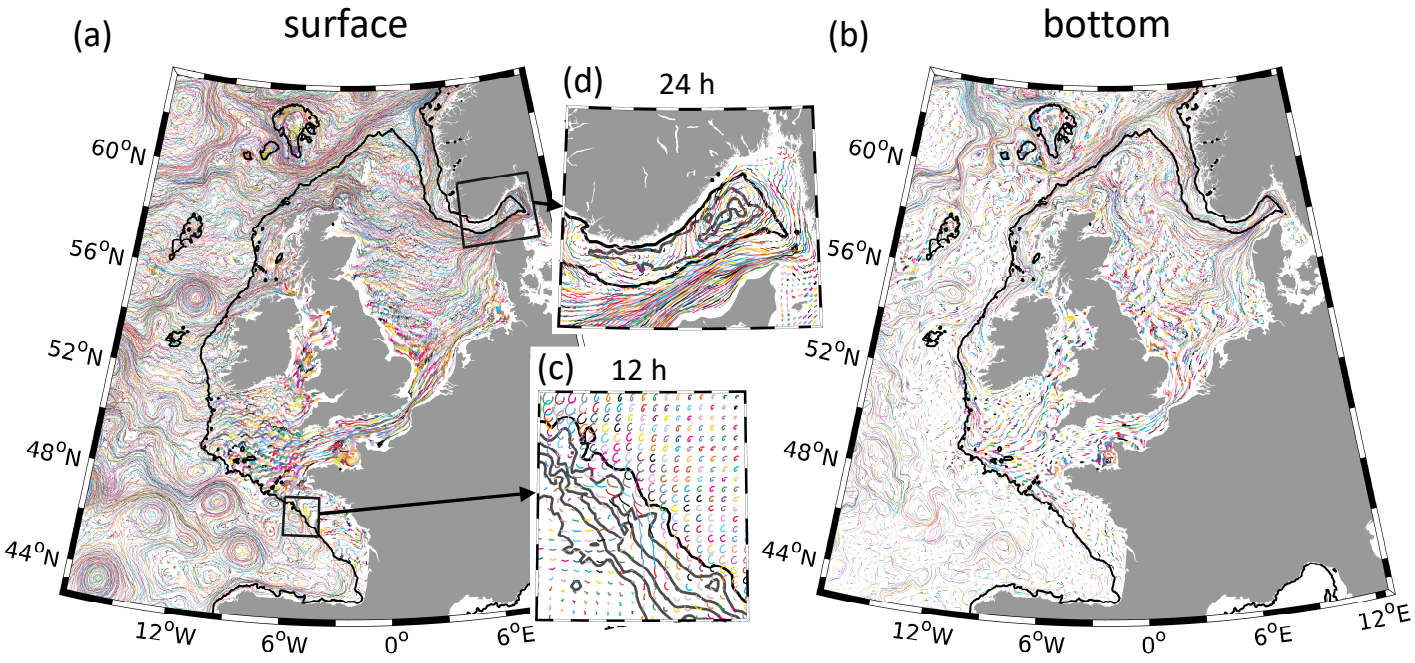

Fig. 3.

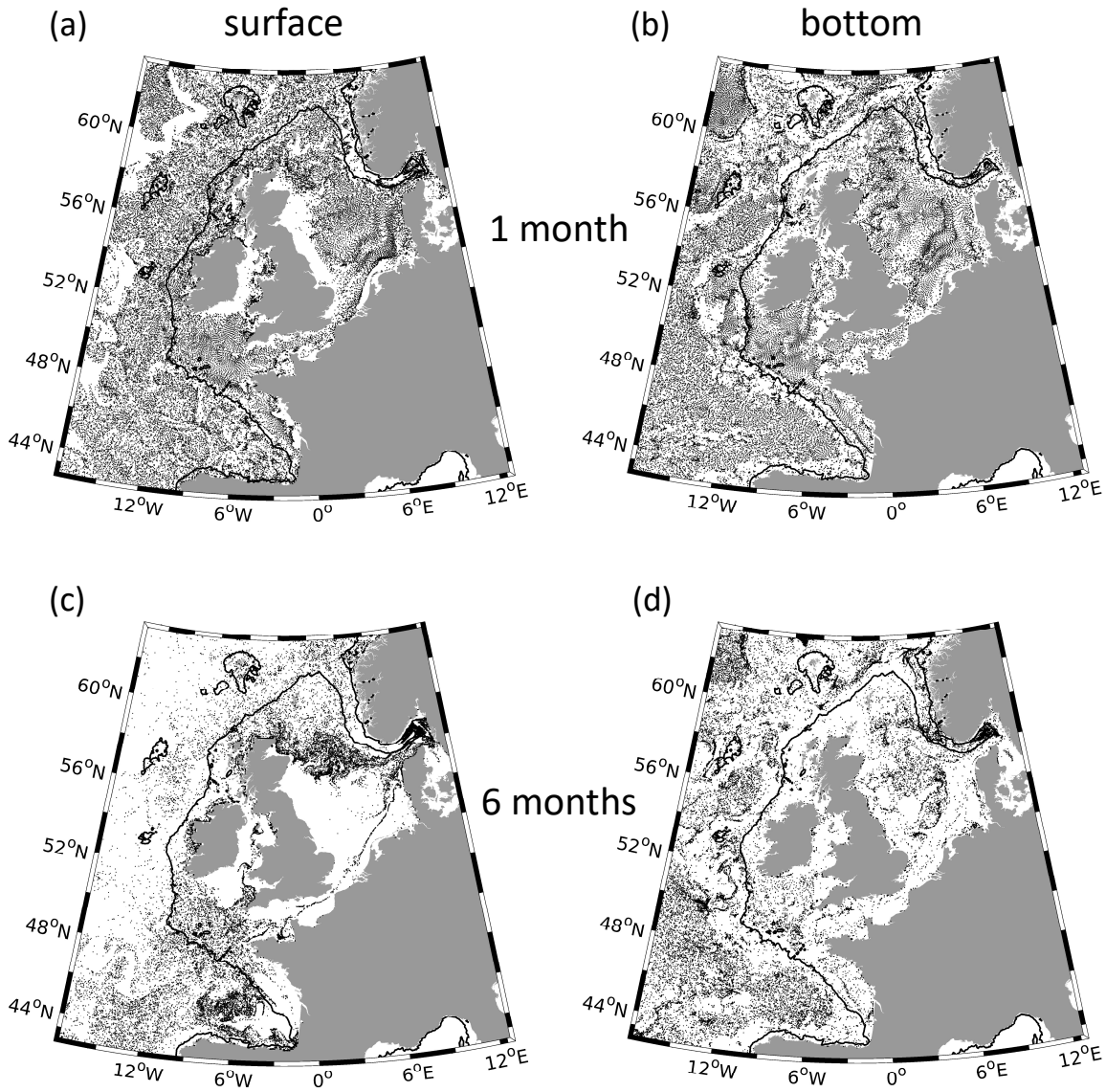
(a)
surface
(b)
bottom
1 month
(c)
(d)
6 months
60°N
56°N
52°N
48°N
44°N
12°W
6°W
0°
6°E
12°E

Fig. 4.

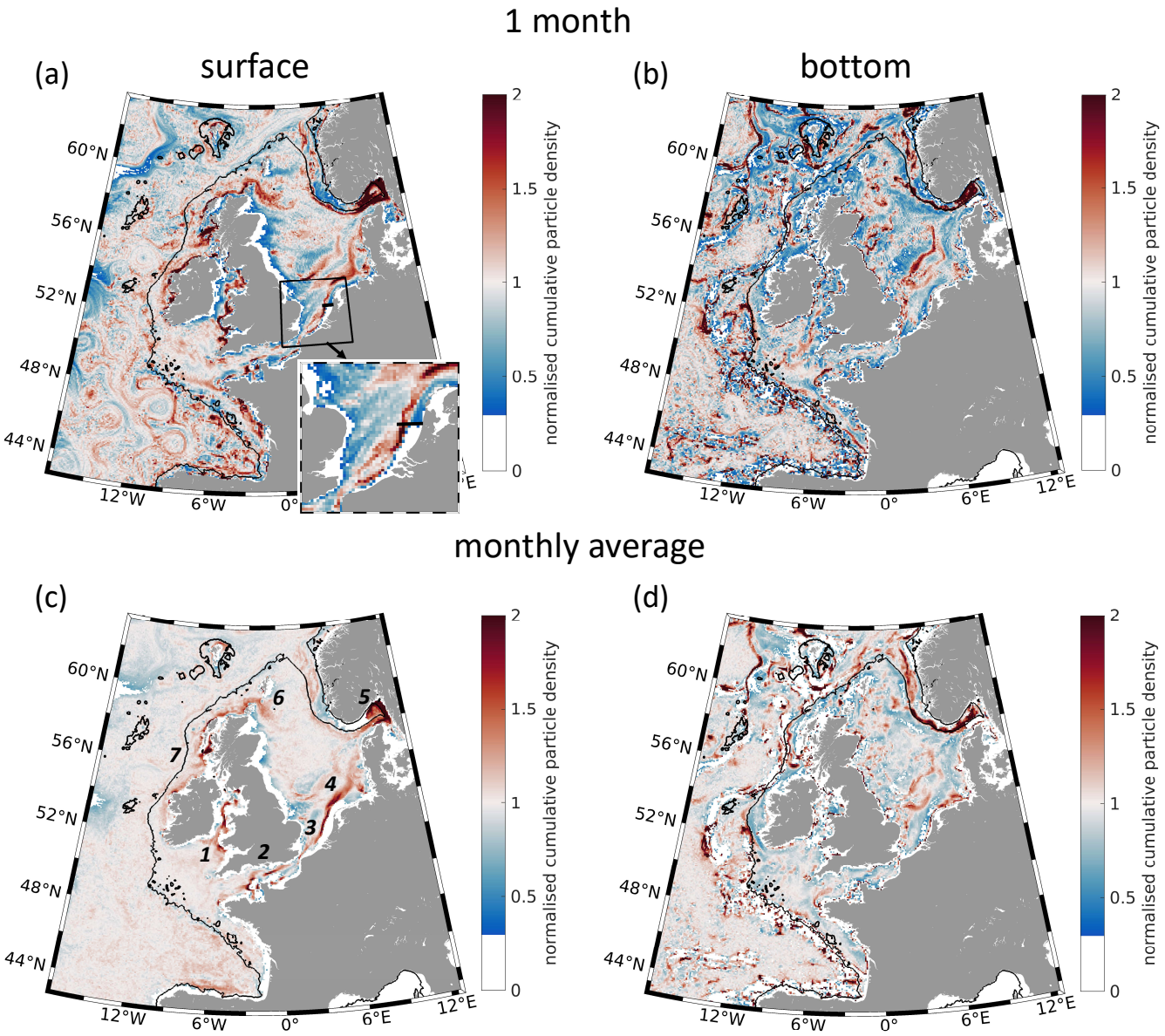
1 month
(a)
surface
(b)
bottom
monthly average
(c)
(d)
60°N
56°N
52°N
48°N
44°N
12°W
6°W
0°
6°E
12°E
normalised cumulative particle density
0
0.5
1
1.5
2
1
2
3
4
5
6
7

Fig. 5.

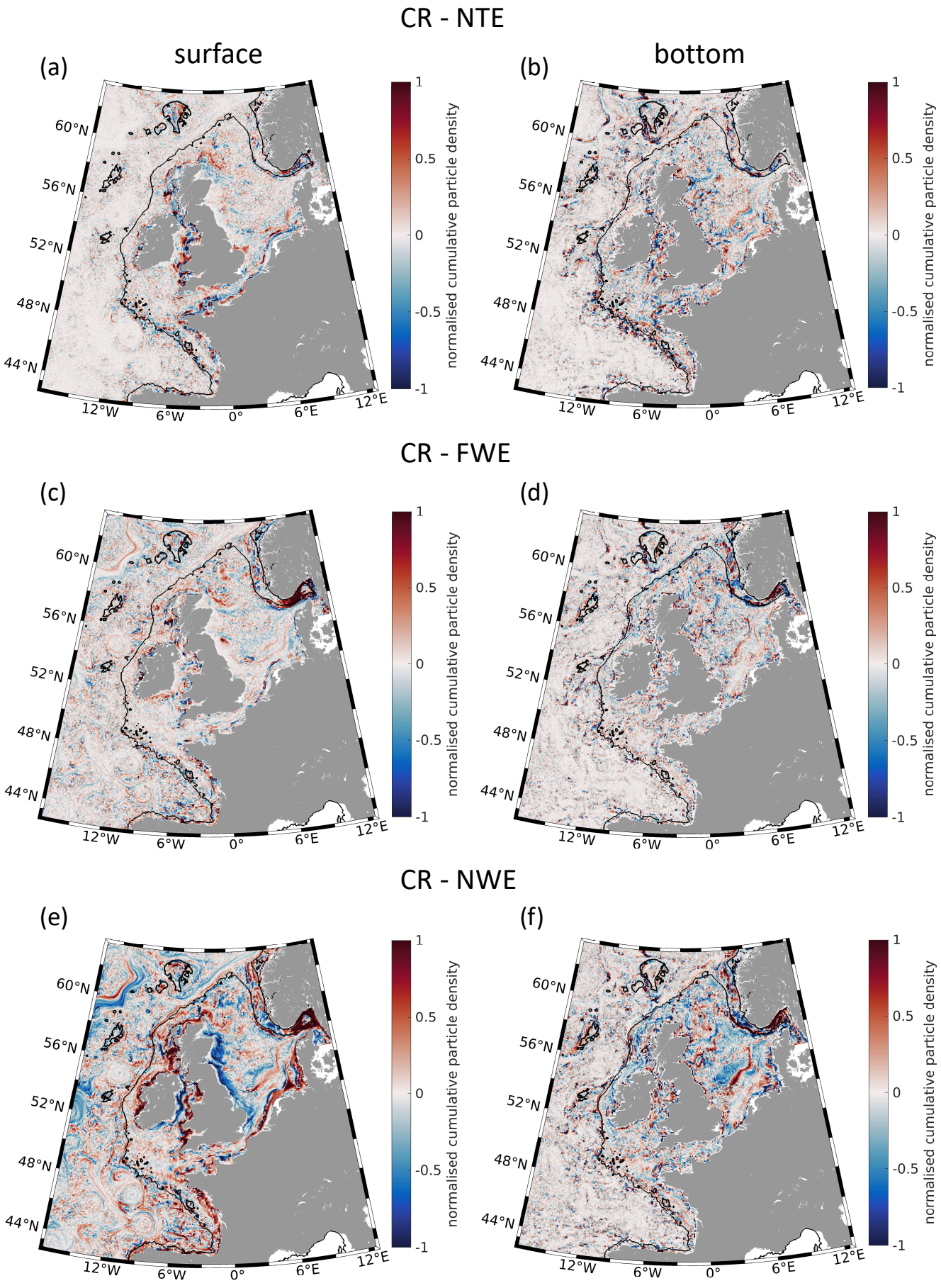
CR - NTE
surface
bottom
(a)
(b)
CR - FWE
(c)
(d)
CR - NWE
(e)
(f)
60°N
56°N
52°N
48°N
44°N
12°W
6°W
0°
6°E
12°E
1
0.5
0
-0.5
-1
normalised cumulative particle density

Fig. 6.

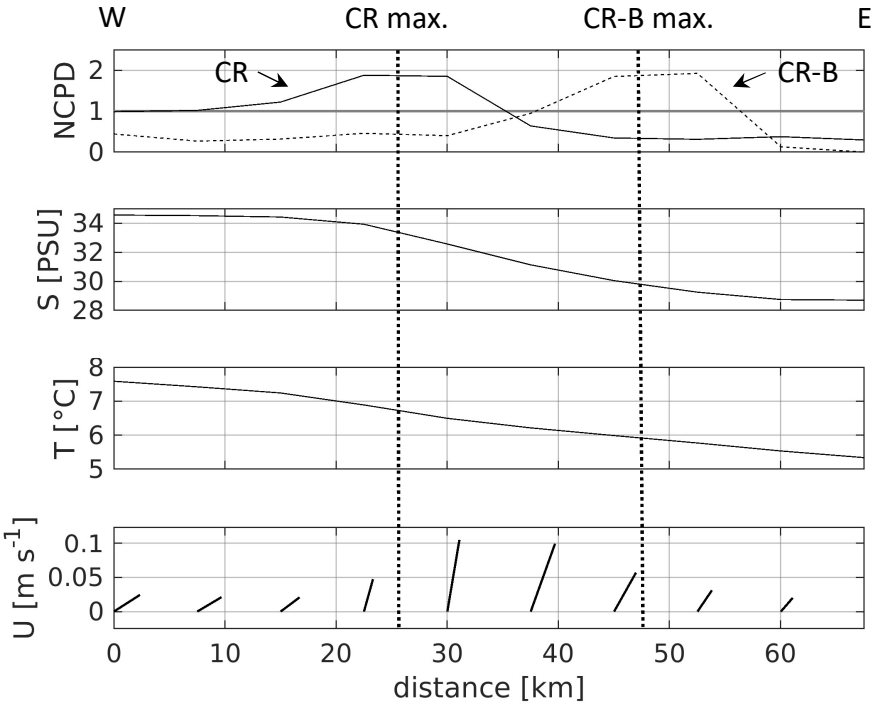

Fig. 7.

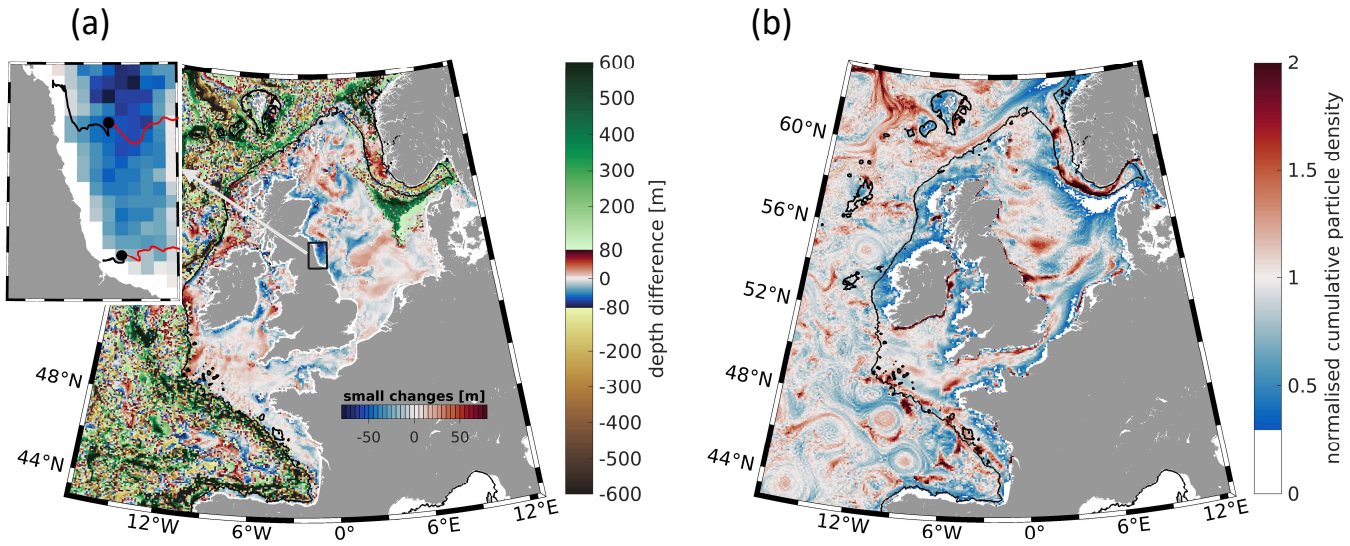
(a)
(b)
600
500
400
300
200
80
0
-80
-200
-300
-400
-500
-600
depth difference [m]
small changes [m]
-50
0
50
48°N
44°N
12°W
6°W
0°
6°E
12°E
60°N
56°N
52°N
2
1.5
1
0.5
0
normalised cumulative particle density

Fig. 8.

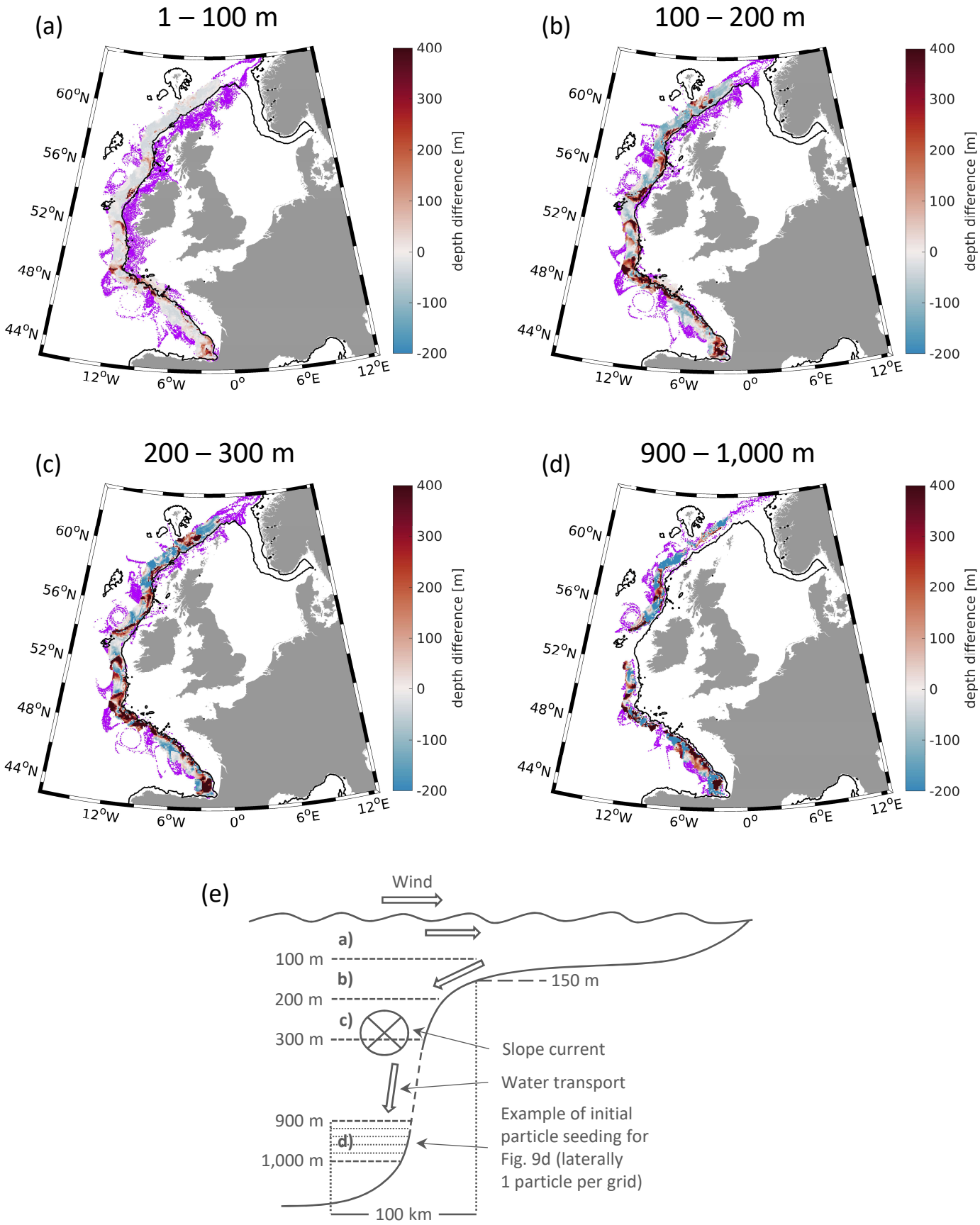
(a)
1 – 100 m
(b)
100 – 200 m
(c)
200 – 300 m
(d)
900 – 1,000 m
60°N
56°N
52°N
48°N
44°N
12°W
6°W
0°
6°E
12°E
400
300
200
100
0
-100
-200
depth difference [m]
(e)
Wind
a)
100 m
b)
200 m
c)
300 m
900 m
d)
1,000 m
150 m
100 km
Slope current
Water transport
Example of initial
particle seeding for
Fig. 9d (laterally
1 particle per grid)

Fig. 9.

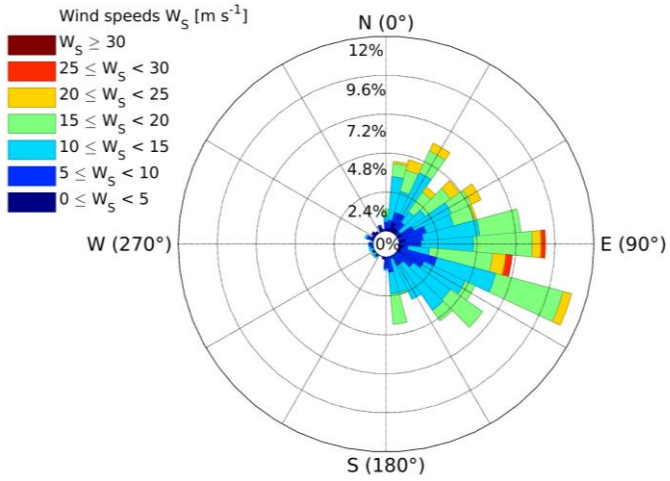

Fig. S1. Wind rose of January 2015 obtained from the model forcing at 53.00° N, 14.94° W. The position of analysis is marked with a black circle in Fig. S3.

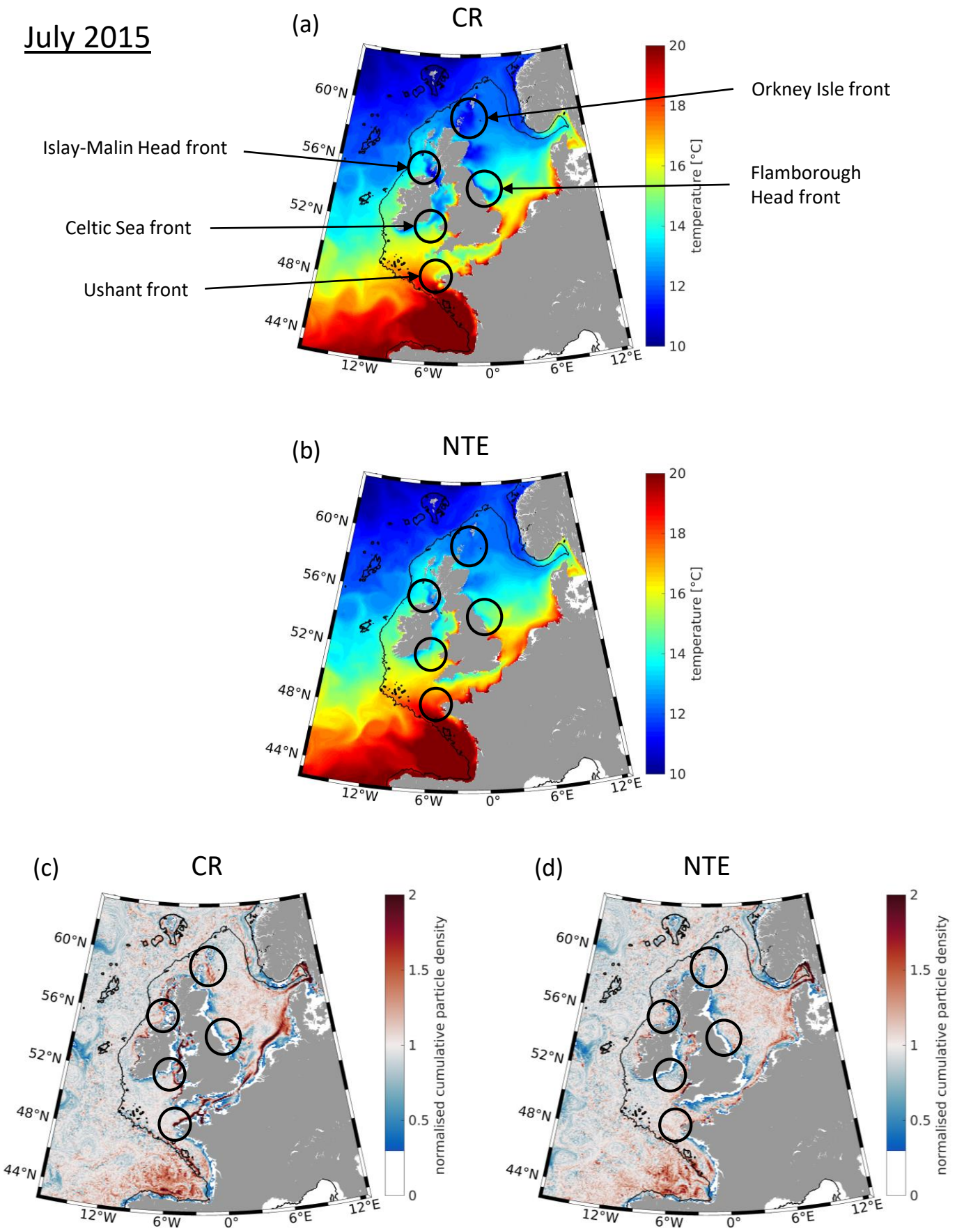

Fig. S2. Typical tidal mixing fronts (black circles) shown in (a) as July 2015 averaged SST distribution in the control run (CR, see Table 1). The respective January SST is shown in Fig. 2e. For comparison, the result of the nontidal experiment (NTE) for same period is shown in (b). NCPD for July 2015 in (c) the CR and (d) NTE.

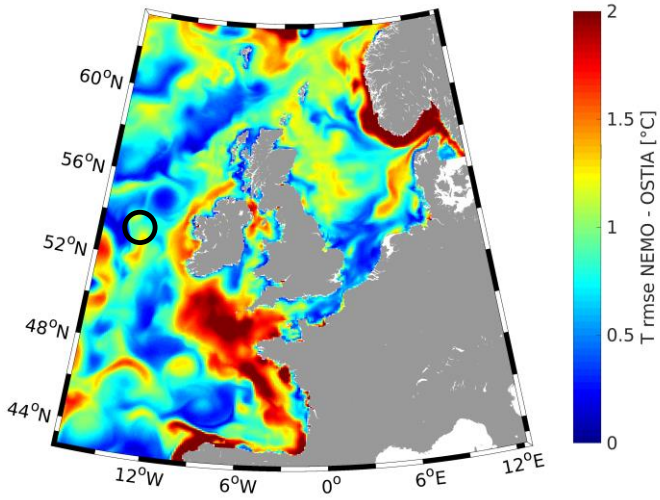

Fig. S3. Root mean square difference (RMSE) of model SST of the control run (CR, see Table 1) and OSTIA data. The black circle denotes the position of wind analysis shown in Fig. S1.

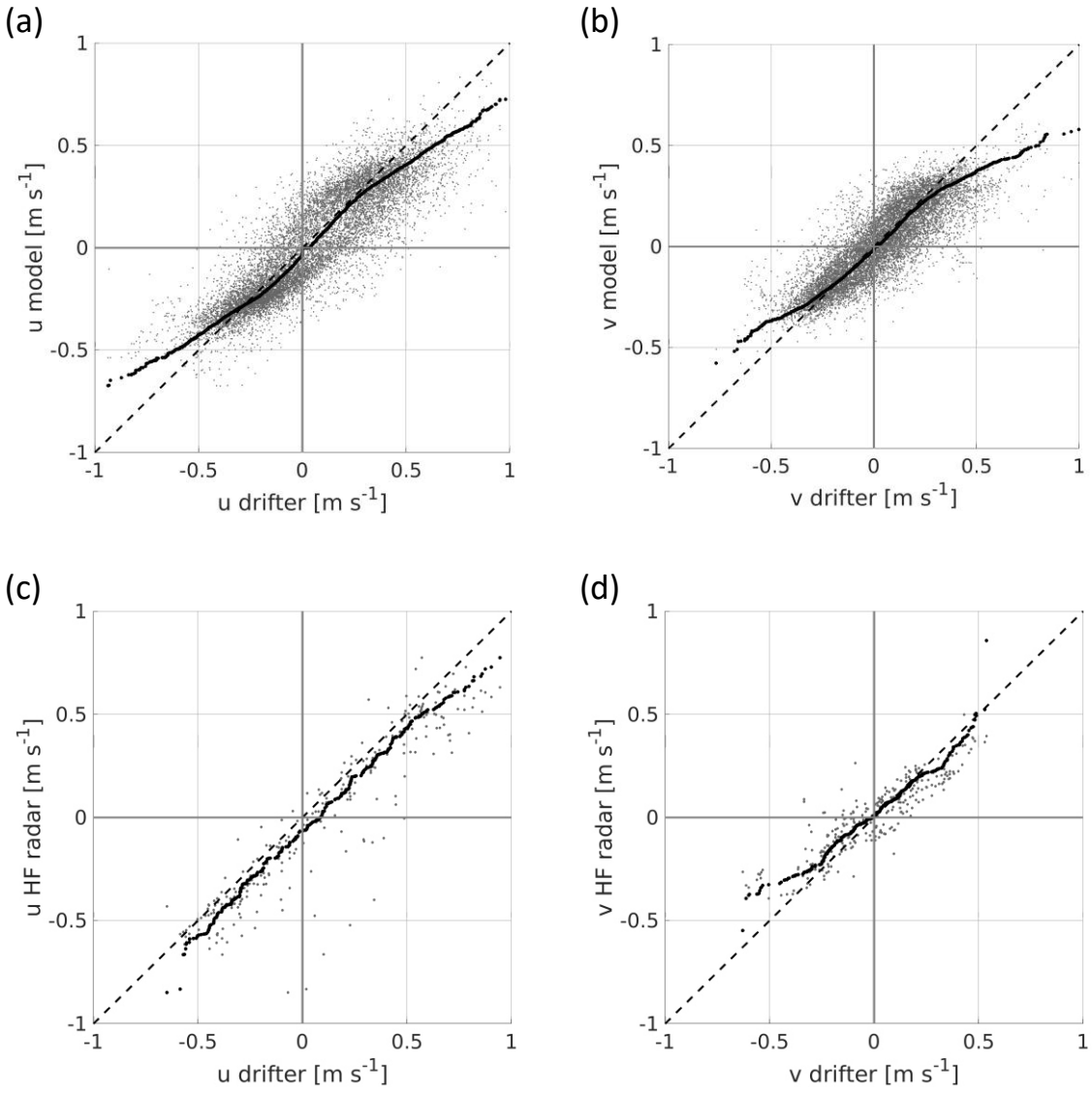

Fig. S4. Scatter plots of (a, b) GPS drifter (May to July 2015) and control run (CR, see Table 1) surface velocities as well as (c, d) HF radar velocities of their (a, c) u and (b, d) v velocity components. Model and HF radar velocities were trilinearly (space and time) interpolated to drifter positions. The dashed line is the diagonal and denotes the optimal dot positions. The black dotted line is the quantile-quantile plot (qq-plot). The amount of available HF radar is less than the drifter data; thus the dots are enlarged. Statistics of each plot are shown in Table 2.

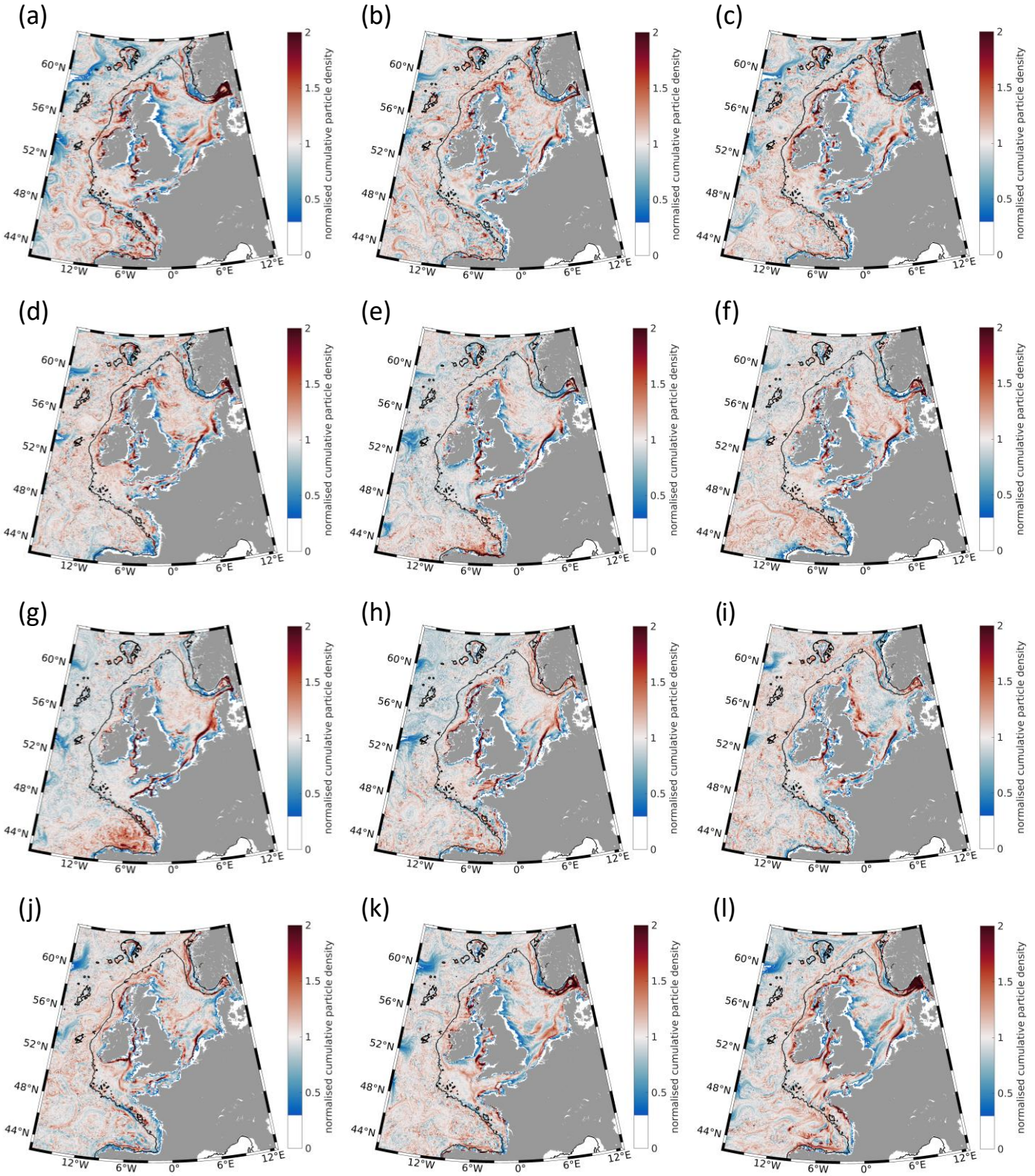

Fig. S5. Tendency of accumulation of surface released particles in the control run (CR, see Table 1) shown as NCPD for every month in 2015; (a) January to (l) December. Note the variability between the single months and compare with its mean in Fig. 5c.

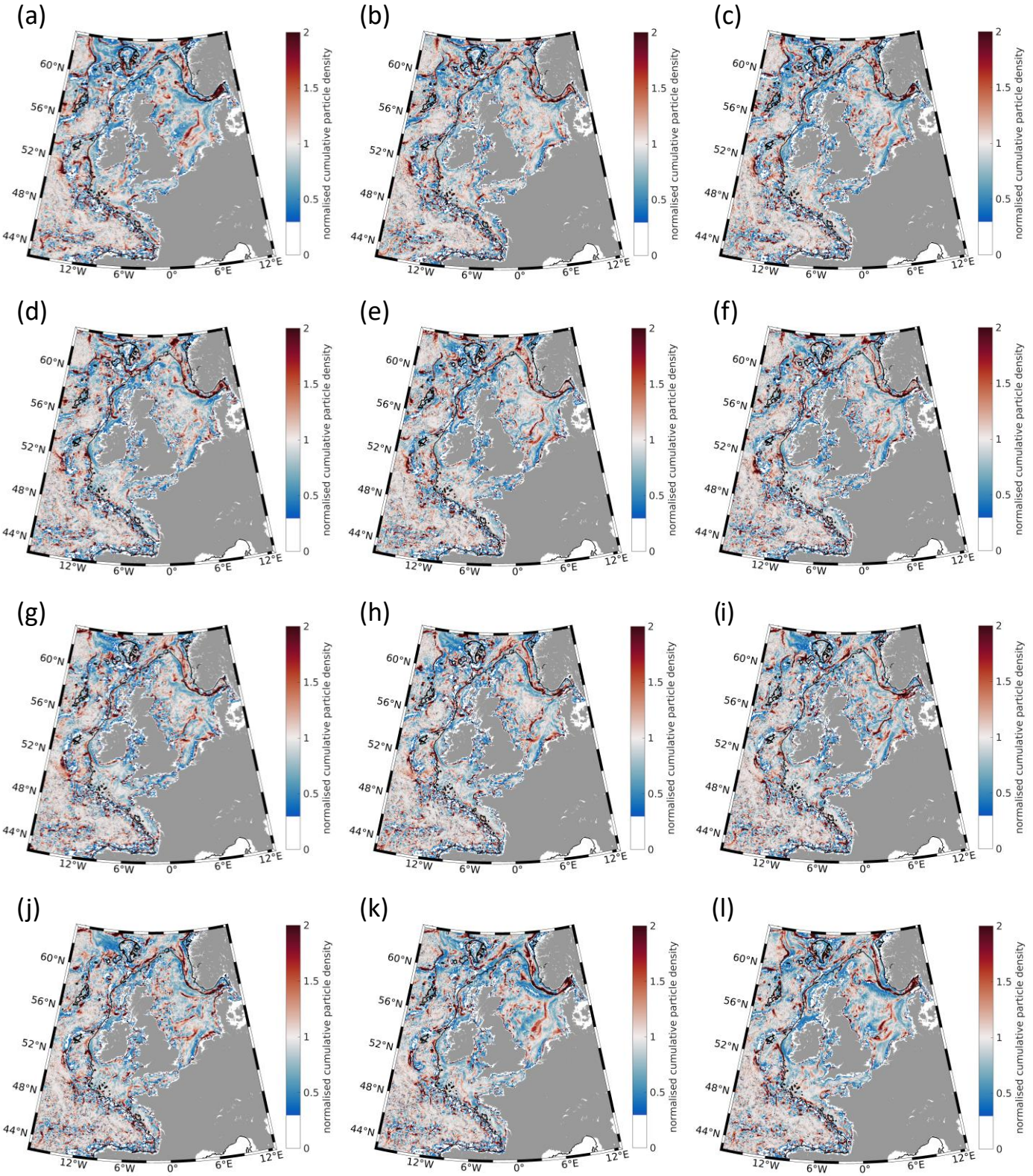

Fig. S6. Tendency of accumulation of bottom released particles in the control run (CR, see Table 1) shown as NCPD for every month in 2015; (a) January to (l) December. Note the variability between the single months and compare with its mean in Fig. 5d.